FINITE ELEMENT ANALYSIS OF PLANETARY GEAR SET FOR WIND TURBINES

A THESIS SUBMITTED TO
THE BOARD OF GRADUATE PROGRAMS
OF
MIDDLE EAST TECHNICAL UNIVERSITY, NORTHERN CYPRUS CAMPUS

BY

YAŞAR ÇAĞATAY KOÇLAR

IN PARTIAL FULFILLMENT OF THE REQUIREMENTS
FOR
THE DEGREE OF MASTER OF SCIENCE
IN MECHANICAL ENGINEERING PROGRAM

JANUARY 2023

Approval of the Board of Graduate Programs

Prof. Dr. Cumali Sabah
Chairperson

I certify that this thesis satisfies all the requirements as a thesis for the degree of Master of Science

Assoc. Prof. Dr. Volkan Esat
Program Coordinator

This is to certify that we have read this thesis and that in our opinion it is fully adequate, in scope and quality, as a thesis for the degree of Master of Science.

Assoc. Prof. Dr. Volkan Esat
Supervisor

Examining Committee Members

Prof. Dr. Eşref Eşkinat
METU NCC – Mechanical Engineering Department

Assoc. Prof. Dr. Volkan Esat
METU NCC – Mechanical Engineering Department

Asst. Prof. Dr. Filiz Alshanableh
NEU - Materials Science and Nanotechnology Engineering Department

I hereby declare that all information in this document has been obtained and presented in accordance with academic rules and ethical conduct. I also declare that, as required by these rules and conduct, I have fully cited and referenced all material and results that are not original to this work.

Name, Last name : Yaşar Çağatay Koçlar

Signature :

ABSTRACT

FINITE ELEMENT ANALYSIS OF PLANETARY GEAR SET FOR WIND TURBINES

Koçlar, Yaşar Çağatay
Master of Science, Mechanical Engineering Program
Supervisor: Assoc. Prof. Dr. Volkan Esat

JANUARY 2023, 71 pages

Planetary gear sets are utilized in various critical applications. Being one of these applications, investigation of wind turbine systems is essential to improve sub-systems such as planetary gearbox, yaw gear, and pitch system under different conditions. In this study, a new finite element model is proposed for obtaining the transient load on the gears of a planetary gearset, and examining the failure types. As an improvement, determination of critical loading scenario for gearset, modeling the blades as a link between the gearset and wind load, and differences between two different beam models are investigated. The model is simulated under reverse load condition which is caused by the sudden change of direction of the wind. The outcome of the simulations shows that the beam model, which takes into account shear deformation, performs within the expected levels according to the literature. Besides, by comparing the outputs of the simulation results, the failure of the gears under an extreme condition is estimated to be due to bending moment on the gear root rather than pitting on the gear tooth surface. As a recommendation for further research, it is suggested to consider reverse load condition in gear designs for wind turbines in order to better understand their behaviour.

Keywords: Planetary gearbox system, Wind turbines, Reverse load condition

ÖZ

RÜZGAR TÜRBİNLERİ İÇİN PLANET DİŞLİ TAKIMININ SONLU ELEMANLAR ANALİZİ

Koçlar, Yaşar Çağatay
Yüksek Lisans, Makina Mühendisliği
Tez Yöneticisi: Doç. Dr. Volkan Esat

OCAK 2023, 71 sayfa

Planet (gezegen) dişli kutuları birçok kritik uygulamada kullanılmaktadır. Bunlardan biri olan rüzgâr türbini sisteminin incelenmesi; gezegen dişli kutusu, kanat yönlendirme sistemi ve rüzgâr dönüş sistemi gibi alt sistemlerin farklı koşullar altında iyileştirilmesi anlamında önem arz etmektedir. Bu çalışmada, bir planet dişli takımının dişlileri üzerindeki zamana bağlı olan yükün elde edilmesi ve hata tipinin incelenmesi için bir sonlu elemanlar modeli önerilmiştir. Önceki çalışmalardan farklı olarak, dişli takımı için kritik yükleme senaryosunun belirlenmesi, kanatların dişli takımı ile rüzgar yükü arasında bir bağlantı olarak modellenmesi ve iki farklı kiriş modeli arasındaki farklar incelenmiştir. Model, rüzgarın ani yön değiştirmesinden kaynaklanan ters yük durumu altında simüle edilmiştir. Benzetim sonuçlarına göre, kesme deformasyonunu dikkate alan kiriş modelinin performansı literatüre uygun olacak şekilde gerçekleşmiştir. Ayrıca, benzetim sonuçlarının çıktıları karşılaştırıldığında, dişlilerin sıra dışı koşullar altında uğradığı deformasyonun dişli yüzeyindeki aşınmadan ziyade dişli kökündeki eğilme momentinden kaynaklandığı belirlenmiştir. İlerideki araştırmalar için, rüzgâr türbinleri kapsamındaki dişli tasarımlarında ters yük durumunun göz önünde bulundurulması davranışın daha iyi anlaşılması adına önerilmektedir.

Anahtar Kelimeler: Gezegen dişli kutusu, Rüzgar türbinleri, Ters yükleme durumu

To my love Sena…

ACKNOWLEDGMENTS

I would like to extend my appreciation to my dear advisor Assoc. Prof. Dr. Volkan Esat for making me all the time motivated, becoming my light along this journey, and sharing time for me. He will always be my idol academically, and personally, too.

In addition to Volkan Hoca, I would like to thank all the instructors that I have been taught by in METU MECH department; Prof. Dr. Eşref Eşkinat, and Assoc. Prof. Dr. Onur Taylan in particular. I have to admit that if I have achieved something today, the contributions which I have gained from them cannot be ignored.

Moreover, my jury member Asst. Prof. Dr. Filiz Alshanableh's comments are also valuable for me as I know that every contribution carries my study one more step ahead.

I am very thankful to my family members: my wife Sena Koçlar, my mother Hatice Koçlar, my father Sinan Koçlar, my brother Muhammed Hüseyin Koçlar. They have always known that I would complete this thesis study for sure even sometimes I thought I would not. They did not have any doubt about my work, always tried to boost my motivation, especially my lovely wife. She has never given up providing her time and energy for me.

After my bachelor years at METU NCC, I am very close to achieving my master's degree again at METU NCC. I am incredibly proud of it. Also, I would like to congratulate my fellow friends who gain their master degrees in these times, and thank them for their full support that I have felt at every struggling time.

This thesis is completely supported by Middle East Technical University Northern Cyprus Campus.

TABLE OF CONTENTS

LIST OF TABLES

TABLES

LIST OF FIGURES

FIGURES

LIST OF ABBREVIATIONS

ABBREVIATIONS	
A	Abnormal
DLC	Design Load Case
DNV-GL	Det Norske Veritas – Germanischer Lloyd
ECD	Extreme Coherent Gust with Direction Change
ECM	Extreme Current Model
EDC	Extreme Direction Change
EOG	Extreme Operating Gust
ETM	Extreme Turbulence Model
EWM	Extreme Wind Model
EWM	Extreme Wind Speed Model
EWS	Extreme Wind Shear
F	Fatigue
FEM	Finite Element Model
IEC	International Electrotechnical Commission
N	Normal
NTM	Normal Turbulence Model
NWP	Normal Wind Profile Model
RNA	Rotor Nacelle Assembly
T & E	Transport and Erection

TFEC	Total Final Energy Consumption
U	Ultimate Strength
UDL	Uniformly Distributed Load
WT	Wind Turbine

LIST OF SYMBOLS

SYMBOLS	
ρ	Air Density
U	Wind Velocity
t	Time
v_*	Friction Velocity
z_0	Roughness Length
κ	von Karman's Constant
φ	Stability Function
a	Moderate Argument
f_c	Coriolis Effect
α	Shear Coefficient
ω	Deflection of Beam
q	Distributed Load
G	Shear Modulus
E	Elastic Modulus
I	Moment of Area

CHAPTER 1

INTRODUCTION

1.1 Background: Wind Energy

In the past few decades, improvements in wind technology have been happening quite rapidly. Since oil and natural gas are finite energy resources, to be able to produce electricity, the idea of adapting renewable energy sources such as wind to our lives carries huge importance [1]. Additionally, in order to decrease the hazards of emissions and their consequences to nature, the subject of how electricity can be produced by renewable energy sources has been studied for many years all over the world. Eventually, wind technology has shown dramatic improvements in about ten years, particularly in US & EU [2]. The total installed capacity in European countries was leading with 153 GW whereas US had 82 GW total installed capacity in 2016 [2]. As an estimation, it will be possible to build 256-397 GW of wind power capacity just in Europe [3], and also 85 and 38 GW of wind power capacity will be available in Germany and United Kingdom, respectively, at the end of 2030 [3]. Figure 1.1 shows the energy intensity improvements starting from 2000 up to 2050. Moreover, the historical and predicted total final energy consumption (TFEC) of renewable in 2015 to around 2050 has been illustrated. By 2050, the contribution to the percentage renewables share of electricity will be about 65% [4].

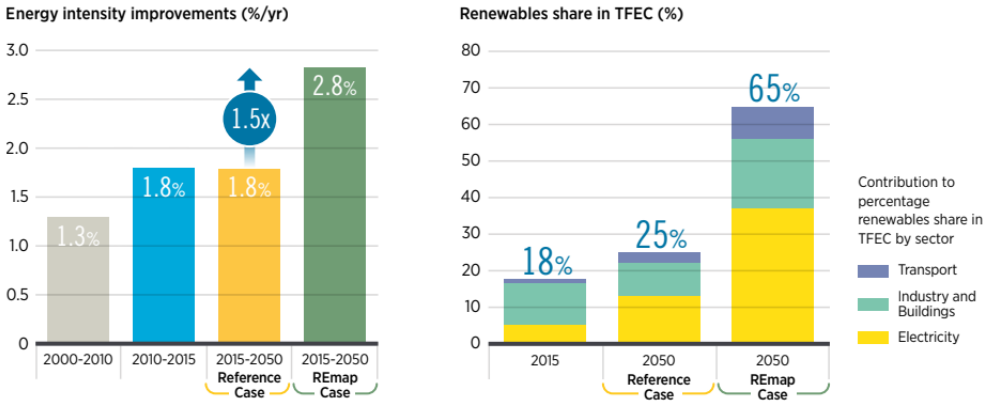

Figure 1.1 Energy intensity improvements and renewables share in TFEC [4]

In Turkey, the most efficient wind power and wind farms are mainly located in the Aegean, Marmara, and Eastern Mediterranean regions, as shown in Figure 1.2 [5]. In 1986, Turkey's first small-scale wind field was established in Izmir-Çeşme region, and it was developed as a prototype with 55kW power. Besides, the first large-scale wind power plant was built in 1998 at the location of Çeşme-Germiyan with 1.74 MW capacity power. The current wind power plant under operation can provide %10 of the electricity needs in Turkey, and this rate is increasing every year. Under global climate change conditions, renewable energy sources such as wind are taking an important role in the economics of every country, for example Turkey, and their carbon dioxide emissions into the atmosphere [6].

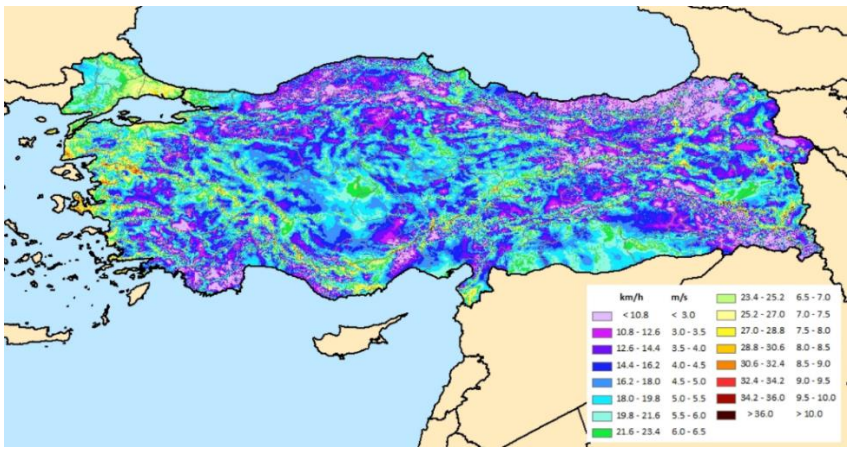

Figure 1.2 Wind power in Turkey [5]

Although wind turbine technology seems very promising, some parts of the wind turbines are needed to be renewed to perform properly during their lifetime. There are various difficulties that the wind turbine industry wants to figure out, for instance, decreasing the cost of wind energy and getting rid of the defects of components such as gears or bearings during its lifetime [7]. Such defects are directly related with the downtime of wind turbines and the rising of maintenance costs.

It is clear that more studies need to be conducted to find out economical and user-friendly solutions. The reliability of wind turbines should be improved so that WT downtime can be reduced and trust in wind turbine technology can be promoted. Lastly, the significance of wind as an alternative and green energy source to oil&gas may be respected more.

1.2 Planetary Gearbox System

Planetary gearbox systems have been extensively used in multiple areas, such as automobile industry, renewable energy, aerospace industry, etc. For instance, in order to increase the rotational speed of the generator of a wind turbine, planetary gearboxes can be placed between the driven rotating blades and the generator. Commonly, a planetary gear set includes a ring gear, a sun gear, and multiple planetary gears. Planetary gears are placed in between sun and ring gear so that, the load in the system is shared among planet gears and torque capability can be improved. Moreover, other advantages of using planetary gearboxes system is high-power density and compact size [8]. Three different types of gear in a planetary gear set are illustrated in Figure 1.3.

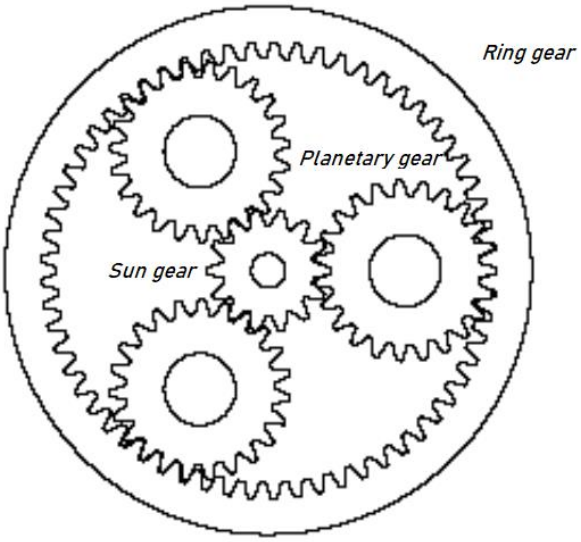

Figure 1.3 Three types of gears in a planetary gear set [8]

There are various categories which are depending on the operation of the system by driving gear. For example, in the case of the ring gear being fixed, the rotational direction of output and input shaft is identical [9]. Therefore, there are two possibilities for the operation in the case of the ring gear being fixed. One of the possibilities is that sun gear becomes an input tool, and the carrier is the output. In that case, a decrease in the speed and an increase in the torque are achieved. Another possibility is that the carrier becomes the input tool, and the sun gear turns as output. Accordingly, the increase in speed and decrease in torque is examined [10]. A summary of all categories can be seen in Table 1.1.

Table 1.1 Planetary gearbox types

Type	*Input*	*Output*	*Purpose*
Fixed ring gear #1	Sun gear	Carrier	Decrease speed and increase torque
Fixed ring gear #2	Carrier	Sun gear	Increases speed and decreases torque
Fixed sun gear #1	Ring gear	Carrier	Reduces the speed
Fixed sun gear #2	Carrier	Ring gear	High driving speed
Fixed carrier #1	Sun gear	Ring gear	Reduces the input speed
Fixed carrier #2	Ring gear	Sun gear	Reversing

In general, rotating components are supported with bearings for planetary gearboxes. In Figure 1.4, A planetary gearbox which composes of four planet gears and a carrier shaft, is assisted by bearings. Rolling element bearing parts are sorted as rollers, inner race, outer race, and the cage to be used for keeping lots of rollers is illustrated in Figure 1.5.

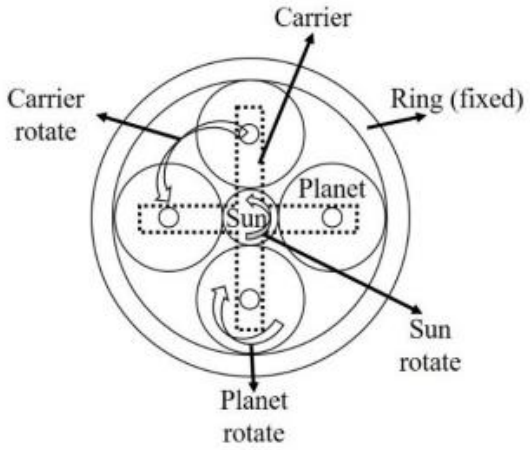

Figure 1.4 Planetary gearbox including four planet gears with the ring gear fixed [11]

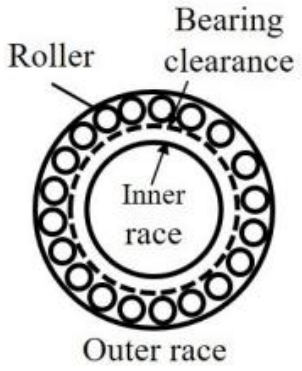

Figure 1.5 Sample rolling element bearing [11]

Due to their complicated structure and potentially carrying heavy loads, these gearboxes tend to experience several defects despite the fact that they are structurally very strong. Tooth chipping, tooth pitting, and tooth cracks can threaten the stability of the planetary gearbox [12]. Extreme loads and material failure lead to cause such tooth cracks as described in Figure 1.6 (a). If the pits arise in the tooth surface, it is called tooth pitting, available in Figure 1.6 (b) and its main reason is long-term tooth contact [13]. Also, there is one more well-known defect for gears that is known as tooth chipping which is the splitting of tooth as shown in Figure 1.6 (c).

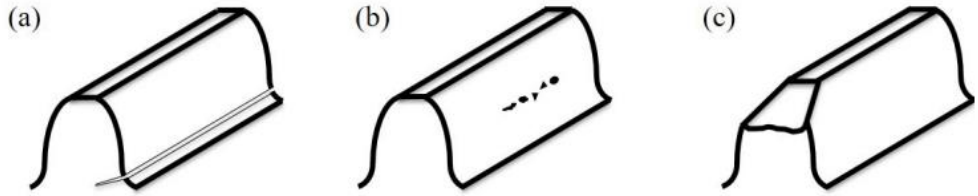

Figure 1.6 Gear tooth defects (a) tooth crack, (b) tooth pitting, (c) tooth chipping [13]

These defects explained above, which are related with tooth damage, are very often encountered. Gearbox defects are recorded as gearbox failures at the rate of 60% [14]. The stability and capability of the planetary gearboxes are affected in a negative way when the tooth is exposed to damage. The sun gear is a significant part of being able to transfer high speed from the input shaft to the generator. Toot crack can be observed if the long-term high-load operation is applied [15]. Many researchers have focused on the defect type of planetary gearboxes.

1.3 Current Challenges

Since people need energy more and more every day, renewable energy sources such as wind power have been expanding in recent years. This expansion leads to growth in the size of the rotor diameter of the wind turbines as well as growth in the number of wind turbines. As it can be seen in Figure 1.7, in addition to this growth in the size of wind turbines, the growth rate is also increasing continuously with the new trend over the years [16]. On the other hand, the renewable energy industry, which is obtained with wind energy, faces many challenges. One of the challenges behind this growth is the design of the components for large-scale wind turbines, and durability becomes an important role for designing components. The gearbox, which is one of the most important parts of the wind turbine, is also the part that has the most challenges [17].

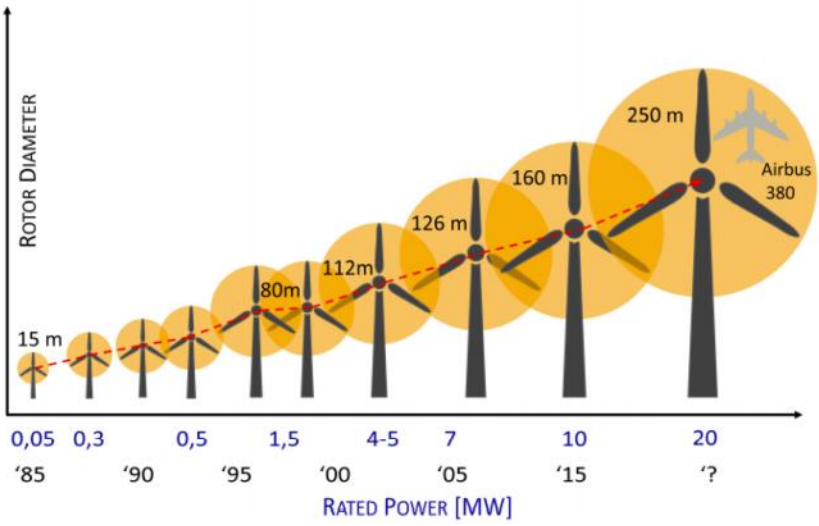

Figure 1.7 Wind Turbine size and rotor diameter changes [16]

By optimization, the components are developed by designers according to different standards, such as IEC-61400 and DNV-GL. Basically, increasing the rotor diameter provides more electricity from wind flow. Nevertheless, this increase in rotor diameter leads to an increase of loads in terms of structural point of view, for instance, extra extreme and fatigue loads on the wind turbine components. The increase in the loading requires stronger designs on the drivetrain of a wind turbine for designers. The drivetrain of a wind turbine is placed where between the generator and blades, the wind energy comes from, in order to generate electrical power for people's needs. Hence, the drivetrain has an important role in wind turbines [18]. In general, there are two common drivetrain categories which are commercial gearbox drivetrain and direct drivetrain in the wind industry. The failures of the drivetrain components, for example gear teeth, bearings are caused by high loads, remarkably due to the size of the rotor diameter of the wind turbine increases. The main challenge of the drivetrain under high load is the durability of the gear teeth. Moreover, failing of the gearbox has a significant effect on the service lifetime of the wind turbines [19]. It causes unexpected shutdown when the turbine is in the operating stage, and it may cause the replacement of components inside the nacelle.

Figure 1.8 Example of the drivetrain of a wind turbine [19]

In general, the failure mode of the gearbox is fatigue type for wind turbines because gearboxes need to withstand the loads coming from wind for a lifetime of around 25 years [20]. However, the failure of the gearboxes under extreme loading should be examined significantly. Since the rotor diameter reaches a very large scale, a situation with the effect of any gust in the wind or the effect of the wind with high turbulences will be more challenging for extreme transient load investigations [21]. Load fluctuations could be introduced additionally as the most critical condition for the gearboxes should be determined and evaluated over these conditions, and these conditions should be determined within the framework of the standards. Basically, wind load fluctuates through the rotor diameter, and this mainly causes a different load scenario for the designers. Such extreme loads do not need to be long-term rather than 25 years fatigue load. Although such extreme loads are very few in number, they should be examined in detail, and the instant time that they may occur on the structure should be considered as well.

Another challenge is the modeling of specific cases when load analyzes are required for a wind turbine component. In general, load analysis is performed separately for the components of wind turbines in the industry, so the effects of these components on each other could be overpassed. Designers need to develop different modeling

approaches for each component and analyze how these designs behave within the overall system. Besides, the effects of each component on each other can be examined with a general aero-elastic coding, but this interaction may be insufficient [22]. Therefore, when analyzes are required on the gears of gearboxes, major loads on the gears must come from the blades through the shaft, and if these loads coming from the blades are modeled correctly, the accuracy of the analyzes on the gear will be increased. In this study, it is aimed to solve these kinds of challenges by modeling the blades and gearbox on the wind turbine in a generalized way.

1.4 Research Objectives

A great amount of research has been conducted on wind turbine systems in order to investigate the challenges and behavior of the sub-systems such as planetary gearbox, yaw gear, and pitch system under different conditions. It has been observed that gearbox failure is one of the most common failing mechanisms for wind turbines. Although wind turbines are exposed to long-term fatigue loads, they are also exposed to extreme transient loads [8]. This study aims to investigate and observe the response of the gears under an extreme transient load for wind turbine gearboxes.

To achieve these objectives, the followings research points will be examined:

1. To create an extreme transient load case, the most critical loading scenario should be selected for a gearbox, and it is important to create the most appropriate wind profile when applying the scenario. There are design load cases in the standard of IEC 61400 that have already been created, examining the situations in the extreme loading sections among these design load cases will guide in finding the most suitable loading condition. Basically, scenarios involving transient loads appear either as scenarios caused by sudden changes in the wind or as scenarios with too much turbulence intensity [22].

In scenarios where there is too much turbulence density, the parts where weakness may occur are usually the blades of the wind turbine, and the blades can prevent weaknesses that may occur with different control mechanisms. However, as the control mechanisms may be delayed in responding to the weaknesses that occur in case of sudden changes in the wind, this loading condition is considered more critical than the other condition [23]. Therefore, one of the objectives of this study is to create a wind profile and examine the gearbox weaknesses that may arise from this profile.

2. To investigate the influence of transient load on the gears, failure type should be determined according to analysis. Basically, planetary gears are generally used for wind turbines, the main reason is to keep the axis of rotation the same. In order to get the best efficiency from the wind, the axis of the blades and the axis of the generator should be aligned [24]. A planetary gear system consists of a central pivoted sun gear, several planet gears, and a ring gear that surrounds both the central and planet gears. As it is known, friction occurs due to the contact of many gears. Also, stresses and distortions can be observed between the surfaces of the gear's teeth with the rotation effect. Consequently, one of the other objectives of this study is examining the effect of interaction between gears, such as pitting and bending moment and which one of them will be more dominant for an extreme transient load case.

3. To perform the analysis according to the created transient load on the gears interaction area, modeling will become essential. Non-uniform remote loads are often used to study the effect of loads such as wind loads on a structural object. Therefore, it is aimed to examine the effect of wind-profiled loads on the blades by using two different beam models and to examine the differences between these two different beam models as a result of the study. Increasing the accuracy of the modeling in line of the results obtained by using different models is among the objectives of this study.

1.5 Outline of the Thesis

The following chapters of the thesis are divided into five chapters, and the explanations of the details in each chapter are listed as follows;

In Chapter 2, an extensive literature review is provided in two main sections, including energy in the wind and design load cases (dlc). Critical points of the energy in the wind section, atmospheric boundary layer and vertical wind profile are presented with introducing two different wind profiles which are logarithmic wind profile and power-law profile. Furthermore, Design load cases section is covered with three sub sections which are load estimation methods, design requirement (IEC standard) and reverse load condition.

In Chapter 3, Modeling of the system is introduced with two different beam models which are Euler-Bernoulli beam model and Timoshenko beam model. Moreover, the finite element model of the system and transient load setup is presented in detail.

In Chapter 4, analyses are carried out using finite element (numerical) analysis software for both Euler-Bernoulli beam model and Timoshenko beam model under reverse load condition in order to observe the response of the gears for a wind turbine gearbox. Findings and comparisons have been summarized with plots and diagrams. Moreover, all the results are discussed in detail.

In Chapter 5, the conclusion of the study has been done and recommendations for the future works are presented.

CHAPTER 2

LITERATURE REVIEW

2.1 Energy in the Wind

Energy in the wind can be defined as kinetic energy from the air motion by relating the mass of air and the velocity of air. The mass flow rate, $\dot{m}$, and any area is dedicated by equation 2.1. Power is energy per unit time. Therefore, wind power can be demonstrated in the equation 2.2. Considering the volume of air passing through an imaginary area which is A, the formula of wind power can be finalized in the equation 2.3 [25].

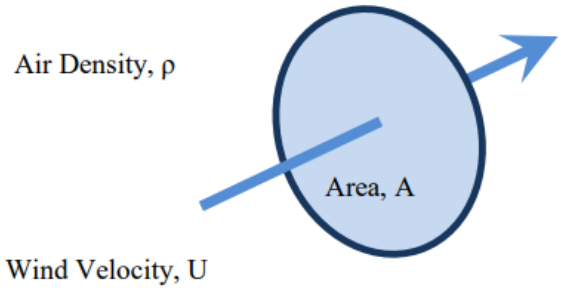

Figure 2.1 Mass flow rate at any area of A [25]

By looking at the derivation of wind energy, it is observed that its energy highly depends on the speed of the wind. Considering the energy formula, it is directly proportional to the cube of the wind speed. Therefore, even the smallest deviations in the wind speed calculation can cause large results in the calculations related to wind energy. In the calculations required for wind turbine load analysis, the wind speed should be reflected as an input to the analysis as precisely as possible. Due to its nature, the wind may not always flow at the same speed or in the same direction. It is very difficult to model the winds that constantly change their speed and

direction, and by performing the models, inputs for wind loads are obtained and analyzes are carried out.

$$\dot{m} = \rho A U \tag{2.1}$$

$$P = \frac{E}{t} \tag{2.2}$$

$$P = \frac{1}{2}(A\rho U^3) \tag{2.3}$$

2.1.1 The Atmospheric Boundary Layer

The atmospheric boundary layer is described as the part of the atmosphere at which the flow domain has a straight impact by the surface of the Earth. Basically, as the wind approaches the Earth's surface, its velocity is assumed to approach zero, and the velocity of the wind has an increasing profile as it moves away from the Earth's surface. The wind in the boundary layer is created by pressure differences at a certain level, and it is necessary to present the wind background in order to determine these wind waves consisting of pressure differences. For example, hydrostatic stability, complex terrain, mesoscale dynamics, etc. are some of the background fields of wind. In addition, this effect remains valid up to 1000 meters above the Earth's surface because the geostrophic zone covers up to 1000 meters above the Earth's surface [26].

2.1.2 Vertical Wind Profile

In order to estimate the wind speed at various hub heights, different wind profiles can be created using the vertical extrapolation methods. The vertical profile of wind flow corresponds to the horizontal wind vector in terms of altitude differences from the earth's surface to a certain level. Since the surface can affect the wind speed in the boundary layer, the wind profile could be changed dramatically from the surface

level. Moreover, most of the methods take roughness and atmospheric stability conditions into account. In general, there are two different vertical extrapolation methods, the logarithmic profile, and the power law profile, which are commonly used in the academic area and wind turbine industry. It has been planned to use the power law profile method for this study.

With the growth of the wind energy field, the sizes of wind turbines are also increasing. Therefore, as the blades of the wind turbines get larger, the area that the blades sweep to generate energy increases. However, while the growth of the blades has a positive effect on energy efficiency, it poses a challenge in estimating the wind profile impacting the blades. Wind turbines with large blades increase the need of a more comprehensive wind profile. For example, the difference between the blades of relatively old wind turbines and the blades of new turbines can be clearly seen in Figure 2.2. It is observed that the turbine with a large blade size in the figure is almost as long as the tower size, which means that it can be as big as 170 meters. In cases where the blade length is very large, the issue of creating a wind profile on the blade should be carefully examined [27,28].

Figure 2.2 (a) new design with large blades (b) old design with small blades [27,28]

In this study, since observing the effect of the wind profile that may occur due to the large blade length is considered as a goal, the wind profile has been created for the occurrence of the reverse load case. Furthermore, one of the main purposes of this study is to determine the critical loads on the gearbox, and in order to overload the gear, it is necessary to create maximum bending moment from the blades and the situation where the deflection is maximum. Therefore, while determining the wind profile on the blades, it is desired to create the profile where the deflection is the highest and the bending effect will be transferred to the shaft. In order to create the reverse load situation most effectively, one of the three blades of the wind turbine should be positioned 90 degrees perpendicular to the horizontal axes of the turbine and above the Rotor Nacelle Assembly (RNA). Because the blade above the RNA creates the bending moment on the shaft as a result of the overload coming from the wind and the deflection in the gear on the shaft at the maximum level. After one blade of the wind turbine is maximized and positioned, the other two blades of the turbine are automatically positioned because the blades have an angle of 120 degrees to each other. Therefore, the reverse load case is best reflected when the wind profile of the other two automatically positioned blades is defined. The approach that the wind flows in the opposite direction of a blade above the RNA and two blades below the RNA best reflects the reverse load case. While creating the wind profile, the wind intensity should also be created on the blades depending on the atmospheric boundary layer. In Figure 2.3, It is observed the position of the blades for reverse load case and the direction of the wind for maximum deflection have been determined.

2.1.2.1 The Logarithmic Profile

The logarithmic law contains the friction velocity "v_*" and roughness length "z_0" which is expressed by the following formula [29].

$$v_z = \frac{v_*}{\kappa}\left[\ln\left(\frac{z - d}{z_0}\right) + \varphi(z, z_0, L)\right] \tag{2.4}$$

Since extrapolation of the wind speed is used, plane displacement is defined as "d" in the formula. Where "κ" is von Karman's constant which is around 0.4. Moreover, "L" (Monin-Obukhov length) is the altitude at which turbulent kinetic energy generation by transmission has the same amount of mechanical turbulence. "φ" represents a stability function and if it takes a negative value it indicates a stable condition, if it gets a positive value it is an unstable condition. The logarithmic profile often loses validity at high altitudes. Therefore, in order to increase the accuracy of this profile, Harris and Eaves (1980) derived a new formula with certain validation coefficients [29].

$$v(z) = \frac{v_*}{\kappa}\left[\ln\frac{z - d}{z_0} + 5.75\alpha - 1.88\alpha^2 - 1.33\alpha^3 + 0.25\alpha^4\right] \tag{2.5}$$

Where the existing altitude is "$z - d$" and "z_g" is the gradient altitude. Therefore, "α" is a moderate argument.

$$\alpha = \frac{z - d}{z_g} \tag{2.6}$$

The "z_g" is expressed as;

$$z_g = \frac{v_*}{6.f_c} \tag{2.7}$$

"f_c" is used to express coriolis effect and it is described as [29];

$$f_c = 2.\Omega.\sin\lambda \tag{2.8}$$

2.1.2.2 Power Law Profile

This law is one of the straightforward methods of estimating the vertical wind profile over the wind turbine height from measurements at a reference level and it is the most commonly used method for the wind energy industry. Basically the formula of power law expression is;

$$\upsilon(z) = \upsilon(z_{ref}).\left(\frac{z}{z_{ref}}\right)^{\alpha} \tag{2.9}$$

Where "$\upsilon(z_{ref})$" and "z_{ref}" indicate wind speed values at reference height and reference height value respectively, usually at 10m. The term "α" is defined as shear coefficient or power shear exponent which is a complex indicator of regional climatology, environmental condition, atmospheric stability, complex terrain and topography [30]. This is obviously observed that the effects of all the parameters have been associated with wind velocity profile, accordingly, their overall impact is transferred in the value of this complex coefficient, "α". With such a complex coefficient, the accuracy of the estimation may be questioned, but many studies have been carried out to prove the accuracy of this method, for example, in a sample site, wind speed estimation was made along the wind turbine using the reference height values without installing wind turbines and using the Power-law method [31]. After the measurements were made (generally for a one year) and the wind turbine was installed specifically for that site, the wind speed data were recorded again at the estimated heights. When these data are compared with the estimated data, it has been observed that this complex coefficient is a realistic estimation method. Moreover, there are large amounts of studies of many researchers (doctoral research and postgraduate studies) and many articles related to this complex coefficient.

In this thesis, the power law profile method is used for estimating the wind speed profile over the blades of a wind turbine. In wind turbines, wind energy hits the blades and creates a rotational effect, and this rotation is transmitted to the generator,

which will produce energy with the shaft at the intersection of the wind turbine blades. Therefore, when creating wind profiles, it is necessary to focus on the profiles on the blades, not on the whole turbine [29]. In order to reflect the reverse load case, different wind profiles should be created on each blade. In addition, the position of the blades should be kept in the most suitable position to cause a reverse load situation. The position of the blades can be seen in Figure 2.3. It will be sufficient to create two different wind profiles for the blades shown in the figure, because the parts of the blade above the RNA and the parts below the RNA will be exposed to two different wind profiles. Due to the placement positions of the wind turbine blades, the two blades under the RNA are expected to have the same wind profile. In addition, it should be taken into account that for the blade above the RNA, the wind acts in a large amount and for the blades under the RNA, the wind acts in a small amount and in the opposite direction.

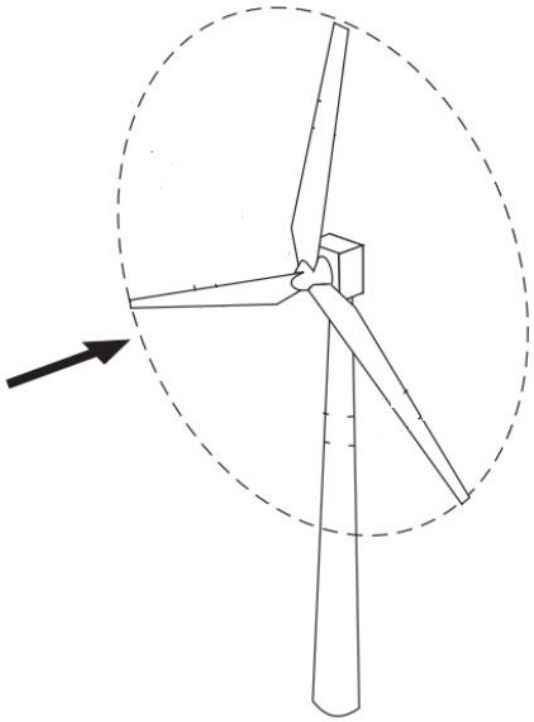

Figure 2.3 Positions of the blades [8]

It is aimed to obtain the power shear exponent by examining articles and theses containing experimental studies, because this thesis does not include any experimental work, it has been progressed by using the power shear exponent as a reference. Furthermore, two different power shear exponent values were found from the literature review, one for the blade above the RNA and the other for the two blades below the RNA. According to Davenport, different wind shear exponents are examined in order to validate wind shear exponent estimations are utilized in load simulations for design of a wind turbine [32]. Performing of several parametric studies have been made in order to simulate wind turbine loads under different conditions of wind shear and turbulence Also, comparisons of the simulated results and standard wind conditions of IEC 61400 are included [33]. In Figure 2.4 taken from this study, comparisons of wind shear exponent obtained with different heights and comparison with the standard are presented. Especially for the wind speed of 0-10 m/s, a very low wind shear coefficient has been noticed [33]. Therefore, these results show us that wind speed is very sensitive under low wind speed estimation and functions could occur. In order to predict a more robust shear coefficient, a nonlinear method has been performed between data from different tower heights. Finally, the wind shear coefficient is fixed to a single value which is "α" = 0.138. In this study, the wind shear coefficient is considered as 0.138 for the blade at above RNA. Moreover, It is important to emphasize that this profile should be used for a blade above the RNA. As an extra point to be considered, while estimating the wind profile, the wind turbine must have a wind speed that needs to be in operation status. Because it is not possible to rotate the shaft that is not in operation status and observe the loads and power. Observing the condition of the gears, which is one of the main purposes of this study, should only be examined when the shaft are rotated at the rated speed.

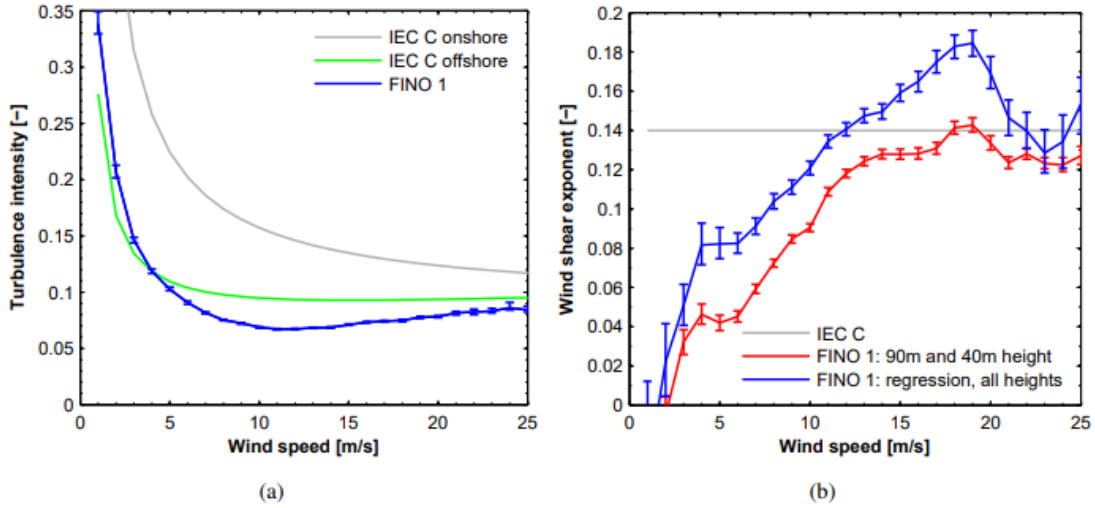

Figure 2.4 The 90th percentile of the measured turbulence intensity and mean value of the measured wind shear exponent [33]

In order to create a wind profile for blades under RNA, the error bars of Figure 2.4 are examined and the best profile has been created for reverse load cases. It is aimed to create a single wind shear coefficient by determining the intervals of the error bars as the intervals with the least errors. Finally, the wind shear coefficient is defined as -0.11 for blades below RNA. Moreover, since the reverse load case reflects the situation where the wind flows in the opposite direction above and below the RNA, the direction of the wind profile to be obtained will be updated in the opposite direction. Roughly, the entire vertical wind speed profile to which the wind turbine blades will be exposed under the reverse load case is illustrated.

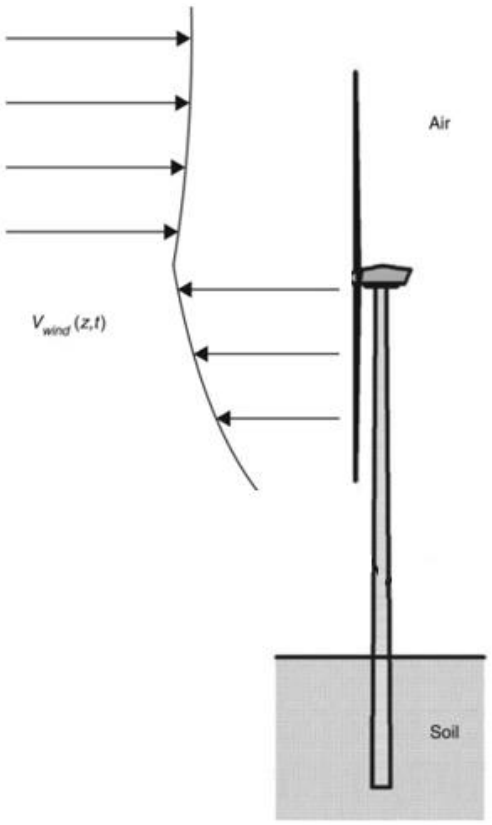

Figure 2.5 Estimated wind profile of the system

2.2 Design Load Case (DLC)

Designers of wind turbines must design in order to provide a long lifetime of operations or extreme conditions, such as more than 20 years, and these designs must be carried out in accordance with certain standards such as International Electrotechnical Commission (IEC). In addition to the loads arising from the internal effects and the nature of the system itself, it is also exposed to loads caused by the sudden change of speed or direction of the wind. This has always been a challenge for designers. Designs are becoming more and more challenging as wind turbines increase in size and are installed in areas with more wind to generate more power. Failures caused by unreliable estimation of design loads or inadequacies in modeling techniques.

2.2.1 Load Estimation Methods

When the wind energy industry was seen as promising, a very detailed structural dynamics model was developed for this industry in the mid-1990s, and after this model was developed, the industry progressed rapidly as a result, the model turned out workhorses in the energy field [34]. Turbulence modeling, stochastic inflow, aerodynamic modeling incorporated with computer coding on the developed model, and estimation for aerodynamic loads can be made in line with these models. This aero-elastic code has been renewed and improved each time, for example by adding effects of pitch and yaw systems [35]. The flow chart of this model, which was created for load prediction and where designers will work on structural components, can be seen in Figure 2.6. Finally, a tool was developed for the designers to work on and the first steps for simulations were taken for the wind energy industry [34].

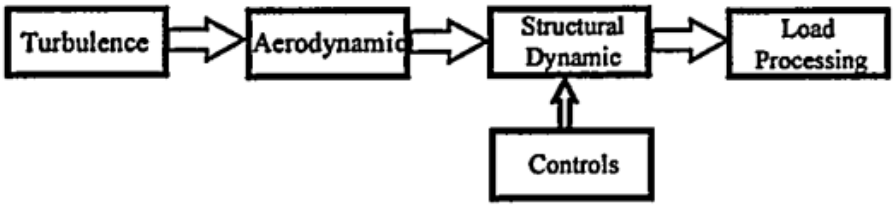

Figure 2.6 Flow chart of turbine model [34]

Basically, the load prediction process covers the duration of time that each wind speed condition has appeared covering the lifetime of the wind turbine. There is a probabilistic approach used for the wind speed density. Turbulence models include variations determined over 600 second time intervals. Loads simulated for 600 seconds and their dynamic response are studied [36]. In these simulations, average wind intervals are determined and simulations are run between these intervals. If it is desired to observe the effect of turbulent wind within 20 life years for the wind turbine, it is necessary to convert low-frequency wind variability to high-frequency wind variability by distributing it over 20 years with the probabilistic density function. By using various cyclic matrices for fatigue load distributions, 600 seconds

of turbulent simulations can be counted, and as a result, the turbulent effect over 20 years is calculated [34].

Extreme types of simulation have different paths followed than for fatigue loads. There are two different sub-models for extreme wind simulations which are the extreme discrete wind speed model and 50-year extreme though 600 second average wind speed model with turbulence [37]. There is a logic that considering the risk posed by extreme loading, all analyzes should be made for these two models and the result should be used in whichever model the highest load result is achieved [34]. However, If the highest load is observed from turbulence, extrapolation of the statics could be needed sometimes. Finally, Prediction of the loads are performed for each component inside the system.

2.2.2 Design Requirements (IEC 61400 Standard)

There is a generally defined standard for wind turbine manufacturers and designers which is The International Electromechanical Commission (IEC 61400). Basically, formulation of the wind speed distribution, safety classes, discretization of the wind condition, state of analysis etc. are covered under design requirements. The main target is to provide a correlative set of models and parameters for wind turbine components in order to reach reliability in the industry [33]. IEC 61400 defined design classes by corporated annual average wind speeds, turbulence density and extreme wind speeds. The Turbulence model and Extreme wind model (EWM) are also included in IEC 61400. On the other hand, It does not define how many turbulence simulations are needed or it does not encourage confidence in estimation of the load levels. There is a table which shows design load cases necessary to analyze a wind turbine [34].

Table 2.1 lists the design load cases in IEC 61400.

Table 2.1 Design load cases [33]

Design situation	DLC	Wind condition	Other conditions	Type of analysis	Partial safety factors
1) Power production	1.1	NTM $V_{in} \leq V_{hub} \leq V_{out}$		U	N
	1.2	NTM $V_{in} < V_{hub} < V_{out}$		F	*
	1.3	ECD $V_{hub} = V_r$		U	N
	1.4	NWP $V_{hub} = V_r$ or V_{out}	External electrical fault	U	N
	1.5	EOG_1 $V_{hub} = V_r$ or V_{out}	Loss of electrical connection	U	N
	1.6	EOG_{50} $V_{hub} = V_r$ or V_{out}		U	N
	1.7	EWS $V_{hub} = V_r$ or V_{out}		U	N
	1.8	EDC_{50} $V_{hub} = V_r$ or V_{out}		U	N
	1.9	ECG $V_{hub} = V_r$		U	N
2) Power production plus occurrence of fault	2.1	NWP $V_{in} < V_{hub} < V_{out}$	Control system fault	U	N
	2.2	NWP $V_{in} < V_{hub} < V_{out}$	Protection system orpreceding internal electrical fault	U	A
	2.3	NTM $V_{in} < V_{hub} < V_{out}$	Control or protectionsystem fault	F	*
3) Start up	3.1	NWP $V_{in} < V_{hub} < V_{out}$		F	*
	3.2	EOG_1 $V_{hub} = V_{in}$, V_r or V_{out}		U	N
	3.3	EDC_1 $V_{hub} = V_{in}$, V_r or V_{out}		U	N
4) Normal shut down	4.1	NWP $V_{in} < V_{hub} < V_{out}$		F	*
	4.2	EOG_1 $V_{hub} = V_r$ or V_{out}		U	N
5) Emergency shut down	5.1	NWP $V_{hub} = V_r$ or V_{out}		U	N
6) Parked (standing stillor idling)	6.1	EWM *50 year recurrence interval*		U	N
	6.2	EWM *50 year recurrence interval*	Loss of electrical powernetwork	U	A
	6.3	EWM *1 year recurrence interval*	Extreme yaw misalignm ent	U	N
	6.4	NTM $V_{hub} < 0{,}7\ V_{ref}$		F	*
7) Parked and fault conditions	7.1	EWM *1 year recurrence interval*		U	A
8) Transport, assembly, maintenance and repair	8.1	To be stated by the manufacturer		U	T
If no cut-out wind speed V_{out} is defined, the value of V_{ref} should be used.					

The table above categorized the applicable Design Load Cases (DLCs) for wind turbines. In

Table 2.1, the DLCs are specified as each design condition by their associated design situation and operational behavior of the system such as control mechanism, protection system and other occurrences [36]. It contains the characteristics cases for assessments of fatigue and ultimate (extreme) loads for the wind turbine components [33].

Basically, design situations of power production cases under normal operation are considered in the 1.x series DLC. In this series, a wind turbine is in the operation position and it is connected to the electric motor. For design calculation, aerodynamic imbalances and maximum mass from the manufacturer must be used. Besides that, fluctuation from theoretical ideal operating scenarios, such as yaw misalignment and control system tracking errors, will also be taken into account when calculating required loads. Design Load Case (DLC) 1.1 and DLC 1.2 are linked together under normal turbulence model (NTM) because the load results from the atmospheric turbulence calculations will be dimensioning when the wind turbine is in operational condition, the extreme loads in the atmospheric turbulent model are examined and observed to be less than the fatigue loads as proof of this. DLC 1.3 contains the type of extreme loading results from the wind condition of the Extreme current model (ECM). DLC 1.4 and DLC 1.5 are linked with potential critical cases such as external electrical fault or loss of the electrical connection.

Power production plus occurence of fault situations or loss of electrical network connection, which causes a shutdown of wind turbine, are considered in the 2.x series DLCs. The design situation includes transient cases. DLC 2.1 contains the control system fault in any extreme cases. DLC 2.2 contains the protection system or preceding internal electrical faults such as generator short circuit. For DLC 2.3, one of the most likely critical wind conditions, Extreme operating gust (EOG), is

considered with external or internal electrical fault including loss of electrical network and combined with abnormal partial safety factor.

Start up cases are considered in the 3.x series DLCs. This series includes both fatigue analysis and extreme types of analysis. The value of the resulting loads is calculated separately for wind speeds, by selecting among 4 or more time points affected by the wind and determining an average value over these values.

Design situation of normal shut down is considered in the 4.x series. Basically, due to the existence of safety and control mechanisms, shutdown situations occur automatically and these situations should be examined for fatigue loads during wind turbine operation and for sudden loads during operation.

Generally, faults in wind turbines can be solved by remotely connecting to wind turbines and resetting the turbine, but in case of an emergency failure, the turbine is instantly stopped by using the emergency shutdown button. Therefore, there is only one design load case for this situation which is 5.1 DLC named as Emergency shut down.

Design situations of parked (stand-still or idling) conditions are considered under fatigue and ultimate types in the 6.x series DLCs. Extreme wind speed model (EWM) takes place in the 6.1, 6.2 and 6.3 DLCs otherwise, 6.4 DLC is examined under fatigue type with normal turbulence model (NTM). Based on the experience gained in the industry, it has been observed that the 6.x DLC series is dimensioning on many load channels in the investigations on the components of wind turbines. Therefore, the characteristic features of the 6.x series DLCs are examined in detail. For example, DLC 6.1 is specifically defined as Parked in 50-year extreme wind and simulation implemented with yaw misalignment of up to ± 15° using the steady extreme wind model or ± 8° using the turbulent wind model. Moreover, DLC 6.2 is specifically defined as parked without grid connection in 50-year extreme wind. Effective yaw misalignment covers ± 180° in the simulations. Another one is DLC 6.3 having detailed description of parked with large yaw error in 1-year wind. In this DLC grouping, DLC 6.4 is the only one having fatigue failure type.

Parked plus fault conditions are considered in the 7.x series DLCs. yaw misalignment of up to ± 15° using the steady extreme wind model or ± 8° using the turbulent wind model is simulated. It is important to notice that DLCs 7.x and DLCs 2.x include fault condition so that, according to the explanation in the IEC standards, the worst scenario of these two situations should be determined and the design loads should be constructed in terms of the loads in this fault condition.

8.x series DLCs are related to transport, assembly, maintenance, and repair. Since it directly affects human health and human life, the safety coefficient is very high in these DLC scenarios and a secondary protection mechanism must be included in these scenarios in order not to cause any disruption to human life.

Moreover, there are two different partial safety factors which are defined as normal and abnormal for each design case.The safety factors that designers should use and include all design load cases are shown in Table 2.2.

Table 2.2 Partial safety factors for loads [33]

Unfavourable loads			**Favourable loads**
Type of design situation			
Normal (N)	**Abnormal (A)**	**Transport and erection (T)**	**All design situations**
1.35*	1.1	1.5	0.9

* For design load case DLC 1.1, given that loads are determined using statistical load extrapolation at prescribed wind speeds between V_{in} and V_{out}, the partial load factor for normal design situations shall be $\gamma_f = 1{,}25$.

If for normal design situations the characteristic value of the load response $F_{gravity}$ due to gravity can be calculated for the design situation in question, and gravity is an unfavourable load, the partial load factor for combined loading from gravity and other sources may have the value $\gamma_f = 1{,}1 + \varphi\varsigma$

2.2.3 Reverse Load Condition

According to the design requirements (IEC 61400) and load estimation methods, the response of a gearbox is going to be examined when exposed to extreme transient loads in wind turbines, which is one of the aims and current challenges of the wind energy industry. Considering IEC 61400, there are many extreme (ultimate) types of load cases that wind turbine components could be affected. However, in this particular study, it is aimed to select only the most critical situation that the gearbox can be subjected to, ignoring all other components of the wind turbine outside the gearbox. It will not be possible to discover the most critical situation that may occur on the gearbox by only examining the standards, so a convergence has been made and the most critical condition that the gearbox can be exposed to under transient loads has been determined as DLC 1.4, since inertial effect of the gearbox from the wind side and also from the operation of the shaft in the gearbox are considered.

The ultimate loads that may occur from the wind are examined in two different ways for severe situations, one of them is caused by the sudden change of the wind and the other is caused by the turbulent wind. As can be foreseen, the critical loads that may occur for gearbox must be caused by the sudden change of the wind because the torque provided by the wind energy will be transferred directly to the gear along the shaft, which can cause a sudden deflection. Due to this deflection, the alignment between the gears can be disturbed and this imbalance can become a problem for the gears of the gearbox. Therefore, after the DLC selection has been determined, a special wind situation has been created specifically for the gearbox analysis, unlike the wind conditions specified in the standards. The name of this wind condition is reverse load condition. The reverse load condition can be considered as the condition which has most deflection of the shaft. Since bending moment and shear force are applied on the main shaft, it is recommended to examine the scenarios that may occur on the gear teeth surfaces such as pitting or bending moment on the gear roots. In order to create this situation, it is necessary to determine the wind profile specially. The gearbox for the wind turbines is located inside the rotor nacelle assembly, which

is called RNA, that is, in the middle of the three blades of wind turbines. Therefore, in order to capture the maximum deflection, the wind profiles above and below the RNA must be modelled in opposite directions to each other. Logically, the greater the moment arm along the wind turbine blades, the greater the deflection will increase. Considering the shear force and bending moment in the connection between the shaft and the wind turbine blades, it is desired to calculate that the moment direction of the blade above the RNA and the moment direction of the blades below the RNA can magnify each other. The magnified bending moment provides the interaction between the gears to a critical level by having the maximum effect on the gearbox located on the shaft. Moreover, considering the location of the boundary conditions on the shaft, bending moment and shear force could cause disturbances in the contact between the gears of the gearbox on the shaft. Therefore, the wind profile can be modified to create this situation and analyzes can be performed. In order to imagine the reverse load condition, Figure 2.7 is attached.

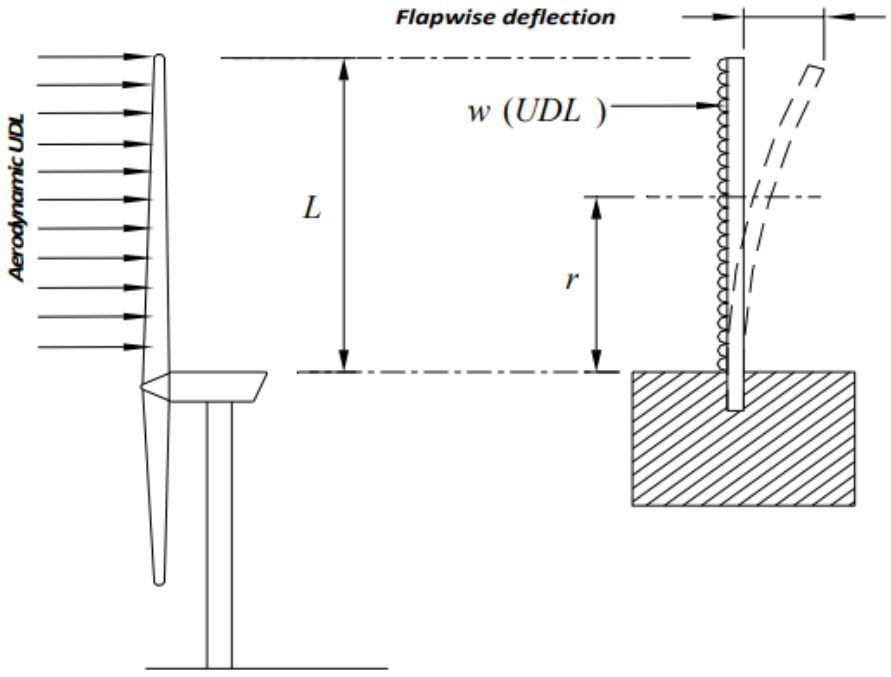

Figure 2.7 Wind turbine loading [38]

CHAPTER 3

MODELLING OF THE SYSTEM

Achieving reliable results and producing efficient solutions in solving a specific problem depends on our approach to the problem and the methods to be used [39]. Wang, Reddy and Lee explain that the methods that can be used are associated with physical theories and formulated mathematical basics. A large number of engineering structures are formed by structural members; for instance, beams, plates and shells where a beam member takes an extensive shape of length-to-lateral aspect ratio and is exposed to longitudinal or transverse forces through its length as well as moments [40]. Therefore, the Timoshenko beam model and Euler-Bernoulli beam model, which are two of the most comprehensive beam models in the literature, were aimed to be used as a part of this research, and the comparisons in the results were enriched. In this study, two different modelling methods have been used for wind turbine blades whose positions and orientations have been discussed in the previous chapter. Due to their position, two different loading conditions occur on the blades under the RNA and above the RNA, and the load distribution to be used for the two different methods will not change. The distribution of load is already created as two different functions in the chapter of Power-Law profile. Then, the static bending problem has been prepared with boundary conditions of cantilever beam and load distributions from wind load. The reason of having a cantilever beam is that the wind turbine blades reflect a structure that extends horizontally and is supported only at one end. Basically, the fixed support section prevents the displacement and rotational movement that may occur there. The free end of the beam has free movement. By solving the governing equations of different beam theories, solutions of bending moment and shear force at the intersection of the blade and shaft are obtained in all the cases. Comparisons are also performed with solutions of bending moment and shear forces on different beam theories.

In the Table 3.1, It can be can seen the blade length and blade mass.

Table 3.1 Properties of the structure

Parameters	Value
Blade length	83 m
Blade mass	16000 kg

3.1 Euler-Bernoulli Beam Model

The Euler-Bernoulli equation characterizes the link between the beam's deflection and applied load. Deflection of the beam is represented by "$\omega(x)$" at the certain direction which is generally in the transverse direction. "q" is a distributed load, and it could be a function of "x" or any other variables. "E" is the elastic modulus of the beam and "I" is the second moment of area of beam's cross section. In general, "EI" is known as flexural rigidity.

$$\frac{d^2}{dx^2}\left(E\mathrm{I}\frac{d^2\omega}{dx^2}\right) = q \tag{3.1}$$

Taking into account the sign convention (right-handed coordinate system) and successive derivation of Hooke's Law, bending moment in the beam can specified as;

$$M = -E\mathrm{I}\frac{d^2\omega}{dx^2} \tag{3.2}$$

Shear force in the beam is;

$$V = -\frac{d}{dx}\left(EI\frac{d^2\omega}{dx^2}\right) \tag{3.3}$$

After beam deflection "$\omega(x)$" has been finalized, bending moment and shear force can be calculated at any section of the beam. The geometry and coordinate system of a cantilever beam and sign convention for shear force and bending moment are shown in Figure 3.1[41].

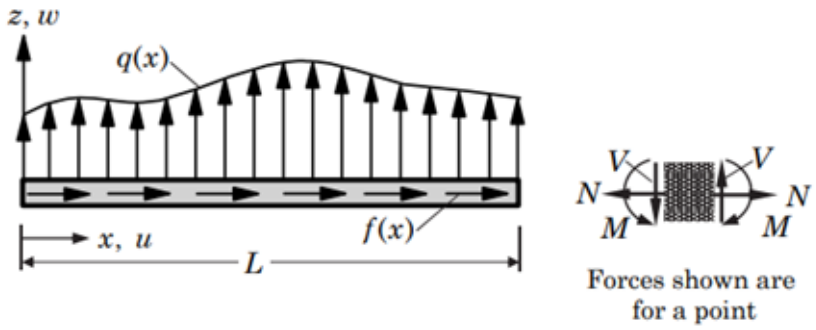

Figure 3.1 The geometry and load sign convention [41]

In order to obtain "$\omega(x)$" Equation 3.1 could be integrated at a certain non-uniform distributed load "$q(x)$". Possible geometric and force boundary conditions are listed in the Table 3.2.

Table 3.2 Conventional boundary conditions for the Euler-Bernoulli beam theory

Type of support	*Geometric B.C.*	*Force B.C.*
Free-free	None	Bending moment and shear force should be known
Pinned-free	$\omega = 0\ and\ \mu = 0$	Only bending moment should be known
Fixed-free	$\omega = 0, \mu = 0\ and\ \frac{d\omega}{dx} = 0$	None

Where a cantilever beam is subjected to a Clamped (Fixed) – Free boundary condition, then the solution in Equation 3.2 and Equation 3.3 are needed to be considered for each segment of the beam. The necessary considerations at the interface of any segments of the cantilever beam are $\left[\theta_x = -\left(\frac{d\omega}{dx}\right)\right]$ are provided from beam continuity equation of deflection and slope and balance of bending moment and shear force [41].

$$\omega_1 = \omega_2, \theta_{x1} = \theta_{x2}, V_1 = V_2, M_1 = M_2 \tag{3.4}$$

Subscripts of "1" and "2" are the segments of the cantilever beam.

3.1.1 Shear Force and Bending Moment Solutions

The expressions for bending moment and shear force for Clamped – Free boundary condition with non-uniform distributed load is illustrated in Appendix A. For "EI" is a constant and "q" is non- uniform distibuted load, the equation of beam is

$$q(x) = a_1x^3 + a_2x^2 + a_3x + a_4 \tag{3.5}$$

$$\frac{d^2}{dx^2}\left(E\mathrm{I}\frac{d^2\omega}{dx^2}\right) = a_1x^3 + a_2x^2 + a_3x + a_4 \tag{3.6}$$

The boundary condition of the beam are

$$\omega(0) = 0, \qquad \frac{d\omega}{dx}\lfloor 0 = 0, \qquad M(L) = 0, \qquad V(L) = 0 \tag{3.7}$$

From Equation 3.7, we have $c_3 = 0$. Use of remaning boundary conditions in Appendix A, shear force and bending moment solutions can be achieved.

3.2 Timoshenko Beam Model

The governing equation of the Timoshenko Beam Theory and Euler- Bernoulli Beam Theory are the very similar to each other. Only difference is Timoshenko beam theory considers rotational inertia effects and shear deformation, provided that for the behavior of thick beams. Therefore, there is an additional term in the formula of generalized displacement [42].

$$\frac{d^2}{dx^2}\left(E\mathrm{I}\frac{d^2\varphi}{dx^2}\right) = q(x) \tag{3.8}$$

The governing equation are the following system of Timoshenko beam theory;

$$\frac{d\omega}{dx} = \varphi - \frac{1}{\mathrm{K}AG}\frac{d}{dx}\left(E\mathrm{I}\frac{d\varphi}{dx}\right) \tag{3.9}$$

When this additional term is lower than 1, The Timoshenko beam theory and Euler-Bernoulli beam theory are equivalent to each other. Since last term is very small amount, It can be neglected;

$$\frac{3E\mathrm{I}}{\mathrm{K}L^2AG} \ll 1 \tag{3.10}$$

By combination of two equation, M and V can be derived [42].

$$E\mathrm{I}\frac{d^4\omega}{dx^4} = q(x) - \frac{E\mathrm{I}}{\mathrm{K}AG}\frac{d^2q}{dx^2} \tag{3.11}$$

$$M = E\mathrm{I}\frac{\partial\varphi}{\partial x}, \qquad V = GAK\left(-\varphi + \frac{\partial\varphi}{\partial x}\right) \tag{3.12}$$

$$GAK\left(-\varphi + \frac{\partial\varphi}{\partial x}\right) = -\int q dx + c_1 = V(x) \tag{3.13}$$

$$E\mathrm{I}\frac{\partial\varphi}{\partial x} = -\int\int q dx dx + c_1 x + c_2 = M(x) \tag{3.14}$$

3.2.1 Shear Force and Bending Moment Solutions

The expressions for bending moment and shear force for Clamped – Free boundary condition with non-uniform distributed load is illustrated in Equation 3.12. For "EI" is a constant and "q" is non- uniform distibuted load, the equation of beam is

$$EI\varphi_x(x) = -\int\int\int q(x)dxdxdx + c_1\frac{x^2}{2} + c_2x + c_3 \qquad (3.15)$$

3.3 Finite Element Modelling

A part of the planetary gear system is modelled and analyzed in ANSYS software which is based on the Finite Element Method (FEM) of analysis. FEM is one of the discretization techniques which dominantly used in the wind turbine industry as well as academic researches. The basic idea of Finite Element Method is the discretization of the complex structure into pieces which should not overlapped elements of the sections. The elements are interconnected with each other in order to reflect the response of every intersection and the solution of model has obtained these discrete elements [43]. In order to create an appropriate model in finite element software, there are certain points to be carried out such as understanding the geometry of the structure, the importance of the material properties and boundary conditions. It has been determined that the shaft of the wind turbine and planetary gear set is modelled in 3D in the SpaceClaim software. Moreover, ANSYS Workbench is used as s solver. The planetary gear set consists of a shaft, a main wheel sun gear, three satellites and a ring gear.

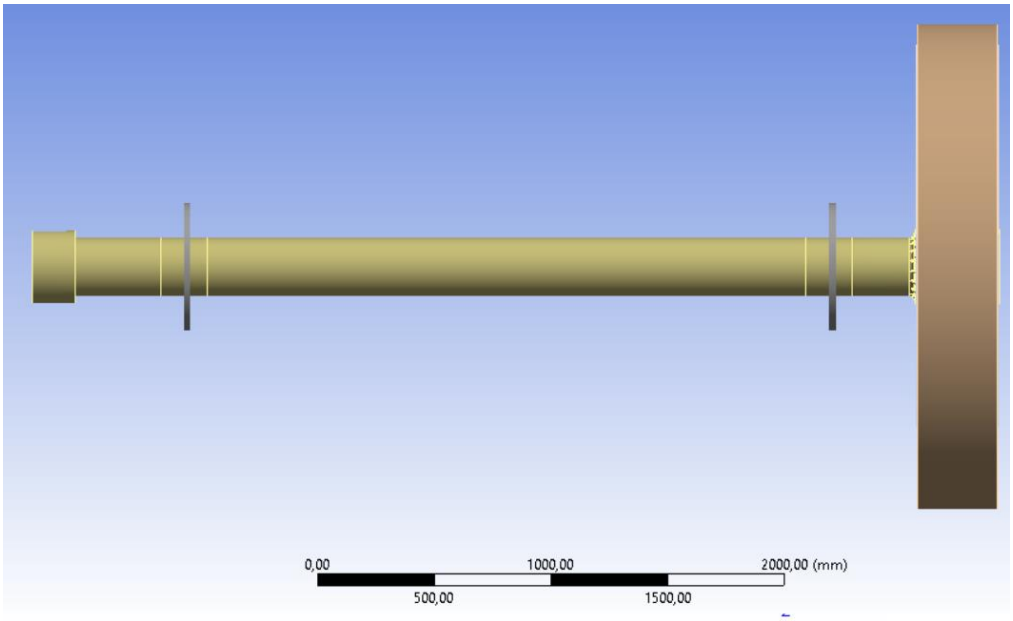

Figure 3.2 3D model of the shaft

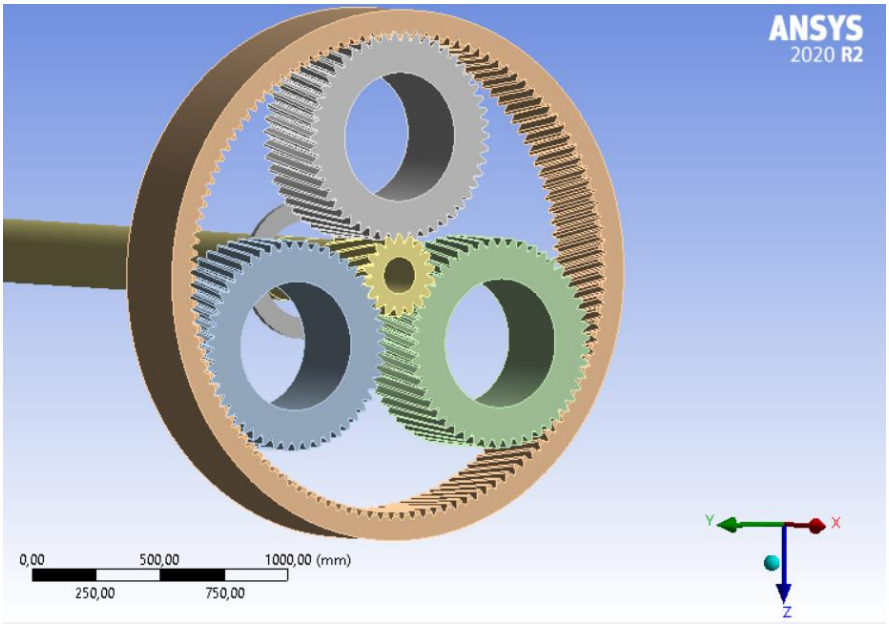

Figure 3.3 3D model of a main wheel sun gear, three satellites and a ring gear

Boundary condition is applied from bearing location since shaft has supported on the bearing locations. Furthermore, shear force and bending moment coming from blade are reflected as initial input in the system. There are three blades and there are six loads (three from shear force, three from bending moment) are applied in total.

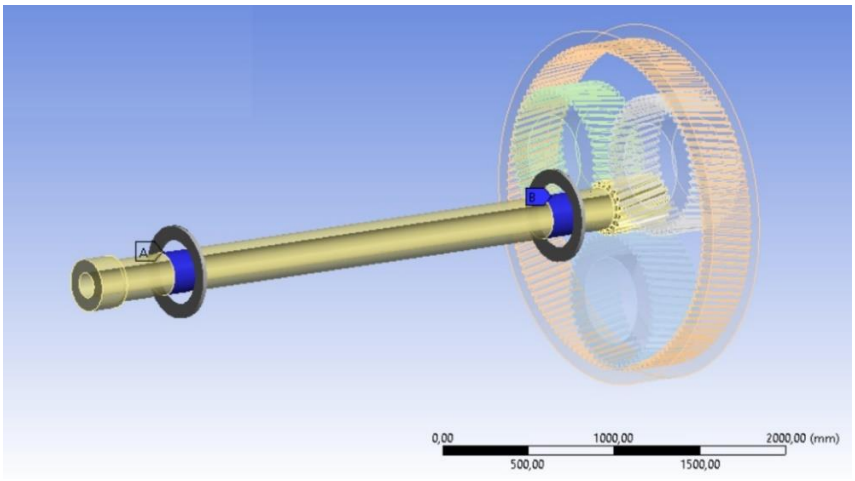

Figure 3.4 Boundary condition of the system

It is possible to observe global stresses and deformations of the geometry using the software. The accuracy of the solution depends on element size, higher element size means that the simulation has been performed with wider margins between the nodes. There are a remarkable number of papers on the topic of element size such as mesh convergency studies or mesh independent solutions. In this study, the solution of every analysis has been performed after the mesh size of the model is accurately arranged. Especially for the contact zone of the gear set is meshed with higher number of elements with smaller mesh sizes as the critical zones for analysis.

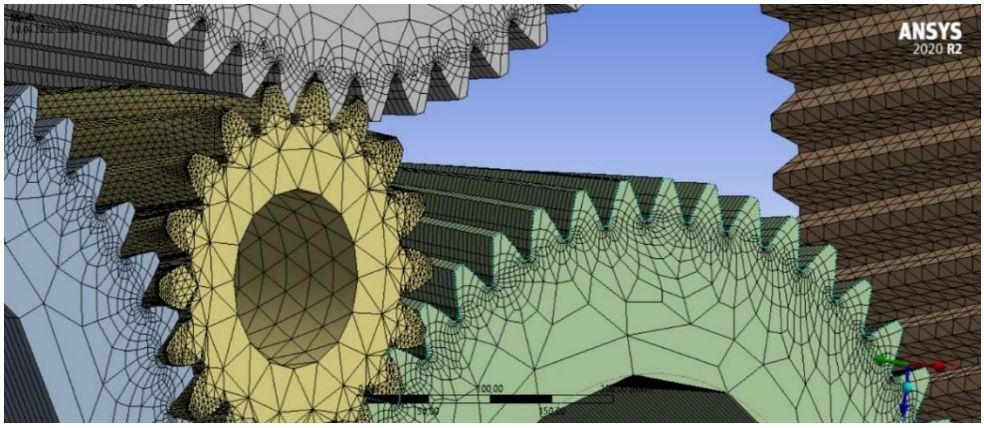

Figure 3.5 Meshed 3D model

In general, the weights of a single wind turbine blade vary between 10-18 tons. The weight of each wind turbine blade used in this study was considered to be 16 tons. Therefore, it was determined that such a large mass could affect the analysis results and blades are modelled as point mass in the finite element software [44].

Table 3.3 Finite element modelling parameters

Parameters	Settings
Formulation of contact	Augmented Lagrange
Type of solver	*Quadratic*
Number of elements	987615
Number of nodes	4644835

Frictional contact is applied between the tooth surfaces of planetary gears, sun gear and ring gear with the behavior of Augmented Lagrange in order to be used to decrease the chatter. Number of elements and nodes are listed in Table 3.3. Material and geometrical properties of gears are presented in Table 3.4 and Table 3.5.

Table 3.4 The material and properties

Material	Properties	
42CrMo4	Density	7,83 g/cm3
	Young's modulus	21,7 kG/mm2
	Yield strength	850 MPa
	Ultimate tensile stress	1000 MPa

Table 3.5 Geometrical parameters of gears

Specification	Parameters
Module (m_n)	14mm
Z_{Sun}	18
Z_{Planet}	52
Z_{Ring}	126
Profile angle	27.1°
Helix angle	8.15°
Face width	325mm

Mesh sensitivity analyses were performed, and von-Mises stress are determined using ANSYS. The overall objective of sensitivity analysis is empirically determining an appropriate mesh resolution.

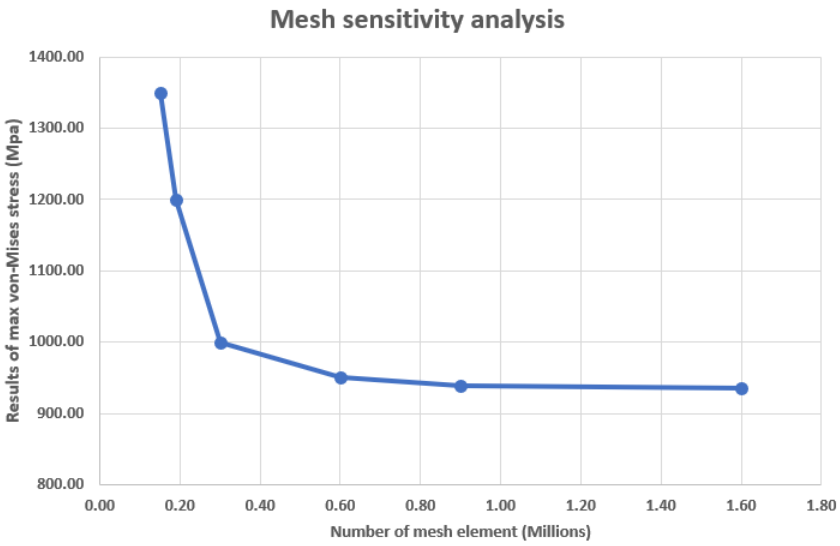

Figure 3.6 Convergence of mesh

3.4 Transient Loading

ANSYS is a commercial finite element software which is used in many areas for the simulation of finite element models. The software includes several analysis types such as static, transient, heat flow and fluid flow. Transient structural analysis refers to the operation of a condition which has a function of time and calculation of effects of loads and internal forces. It is used to perform the dynamic response of a structure with a certain time varying input. The wind load acting on the structure at different instances and it is needed to be considered. Moreover, there are extra components such as shaft, which rotates when wind load is affecting on the structure. Therefore, a complete transient structure analysis provides the most accurate solution for this study. Rotational time varying input is implemented in the transient analysis for the rotation of the shaft. Since shaft is connected to the wind turbine blades, it has the same amount of period speed as the rotation speed of the blades. Wind speed mainly determines the amount of rotation in the wind turbine blades. The wind turbines are designed to operate under a certain range of wind speed. This range depends on the type of the size of the wind turbine. For example, for the wind turbine producing 4MW or 5MW with a rotor diameter of 145m or 170m, this range has been determined as 3m/s to 25m/s [38]. In addition, this range is related to the efficiency of the wind turbine. Moreover, there is a certain speed which is called rated wind speed. Basically, wind turbines are able to operate as their maximum capacity at the rated wind speed. Therefore, it is implemented with the time variable to analyze the rotational speed in the rated wind speed state.

CHAPTER 4

RESULTS AND DISCUSSION

In the previous chapters, modeling of a wind turbine blades with two different beam methods and obtaining the load distribution that may arise from the wind on these wind turbine blades, as well as simulations on the 3D model are explained in detail. In this section, formation of the wind profiles to be reflected on the beam models, the differences between the beam model results and the outputs of the simulations are presented and discussed in line with the standards.

As mentioned in Chapter 2, wind profiles were created using the power law method, which is the simplest of the estimation methods and the most useful for high altitudes. The wind profile can be defined using the power law method as a function that depends on a reference altitude and velocity variables. The input of this function is the height, z, that the wind profile will affect. The wind shear coefficient is a constant and it is taken from literature. It is decided as 0.138 for the blade at above RNA and -0.11 for the blades at below RNA. The wind speed at the reference height was also determined as another constant in the formula. Table 4.1 shows the basic parameters, which define the wind turbine classes [33].

Table 4.1 Basic parameter for wind turbine classes

Wind turbine class	I	II	III	S
V_{ref} (m/s)	50	42.5	37.5	Values specified by the designer
V_{ave} (m/s)	10	8.5	7.5	
A Iref (-)		0.16		
B Iref (-)		0.14		
C Iref (-)		0.12		

According to the three wind turbine classes specified in the standards and the wind shear coefficients taken from the literature, wind profiles were created. Figure 4.1 and Figure 4.2 show the variation of the wind profile along the tower height of 120 meter. It can be clearly concluded that the change in the wind profile increases and decreases in direct proportion to the reference wind speed specified in the standards. Therefore, the reference wind speed can be selected according to the wind classes specified in the standards or a more suitable wind profile can be created by determining the reference wind speed together with certain field measurements.

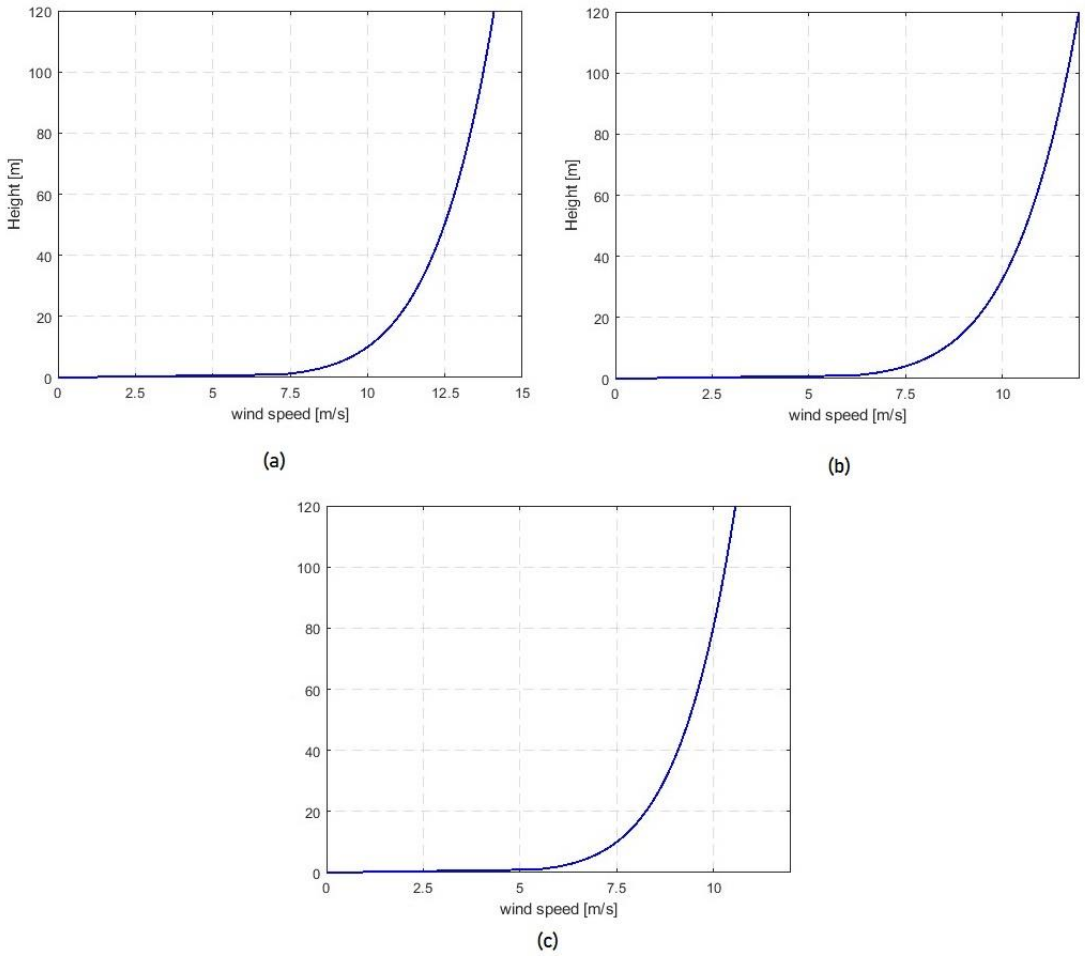

Figure 4.1 Wind speed profile along tower height of 120m with 0.138 wind shear coefficient (a) $v(z_{ref}) = 10\ m/s$, (b) $v(z_{ref}) = 8.5 m/s$, (c) $v(z_{ref}) = 7.5\ m/s$

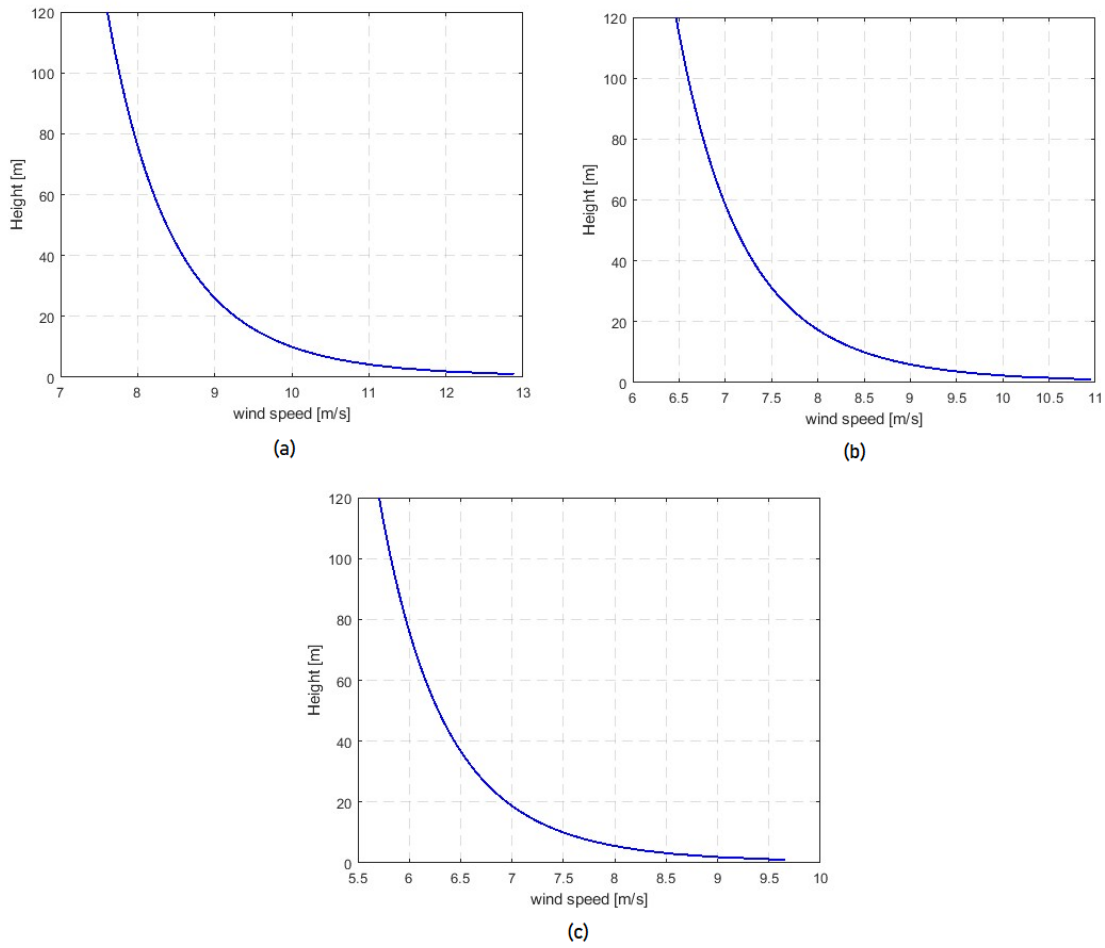

Figure 4.2 Wind speed profile along tower height of 120m with -0.11 wind shear coefficient (a) $v(z_{ref}) = 10\ m/s$, (b) $v(z_{ref}) = 8.5 m/s$, (c) $v(z_{ref}) = 7.5\ m/s$

By comparing Figure 4.3 and Figure 4.4 or because the wind shear coefficient is in the form of exponential, the effect of the wind shear coefficient on the function will not be linear. Generally, exponential functions are used for things involving rapid growth. Therefore, wind profiles were created to cover 10% below and 10% above the wind shear coefficient and these profiles were used in the calculations to be made by beam methods. Figure 4.3 and Figure 4.4 shows differences of wind profiles when %10 margin have been applied on the wind shear coefficient.

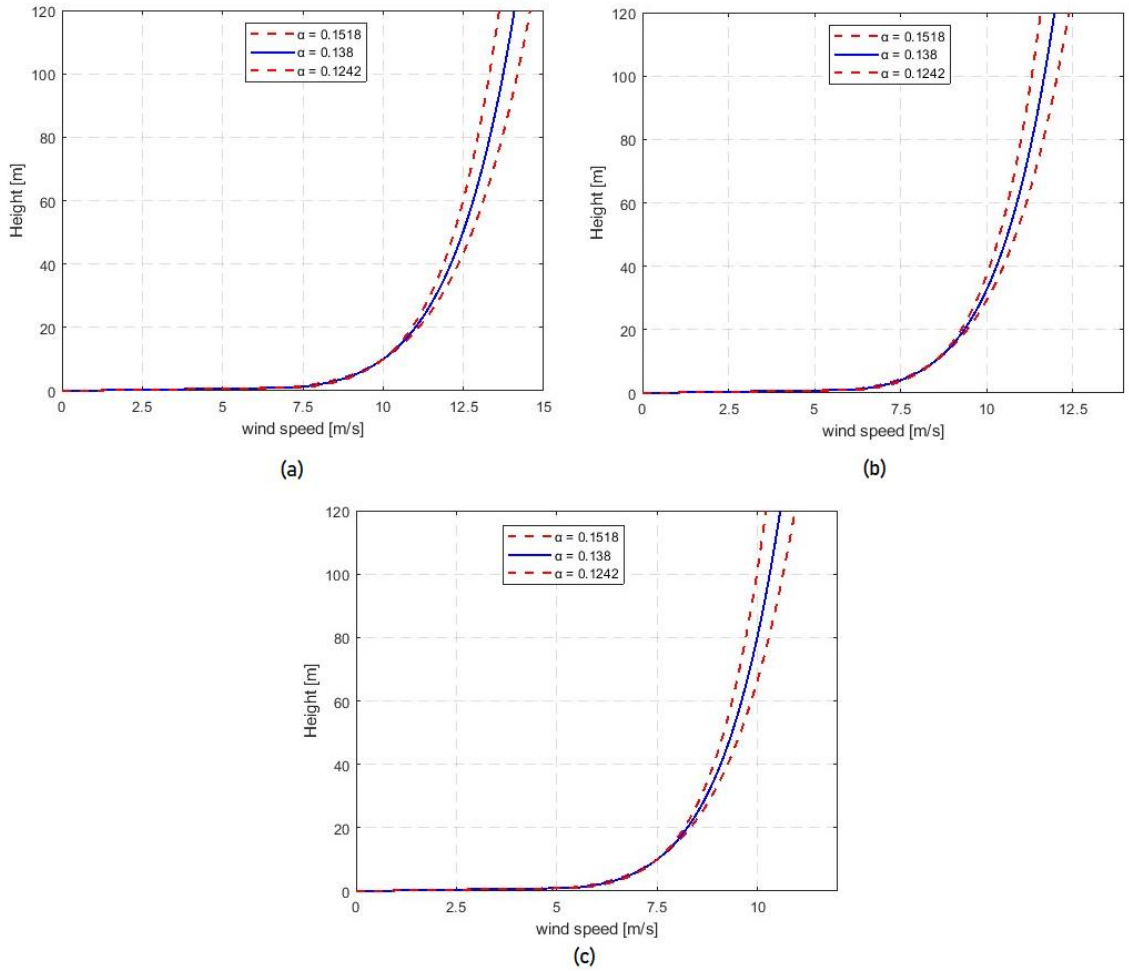

Figure 4.3 Wind speed profile along tower height of 120m with 0.138 wind shear coefficient and %10 margin (a) $\upsilon(z_{ref}) = 10\ m/s$, (b) $\upsilon(z_{ref}) = 8.5 m/s$, (c) $\upsilon(z_{ref}) = 7.5\ m/s$

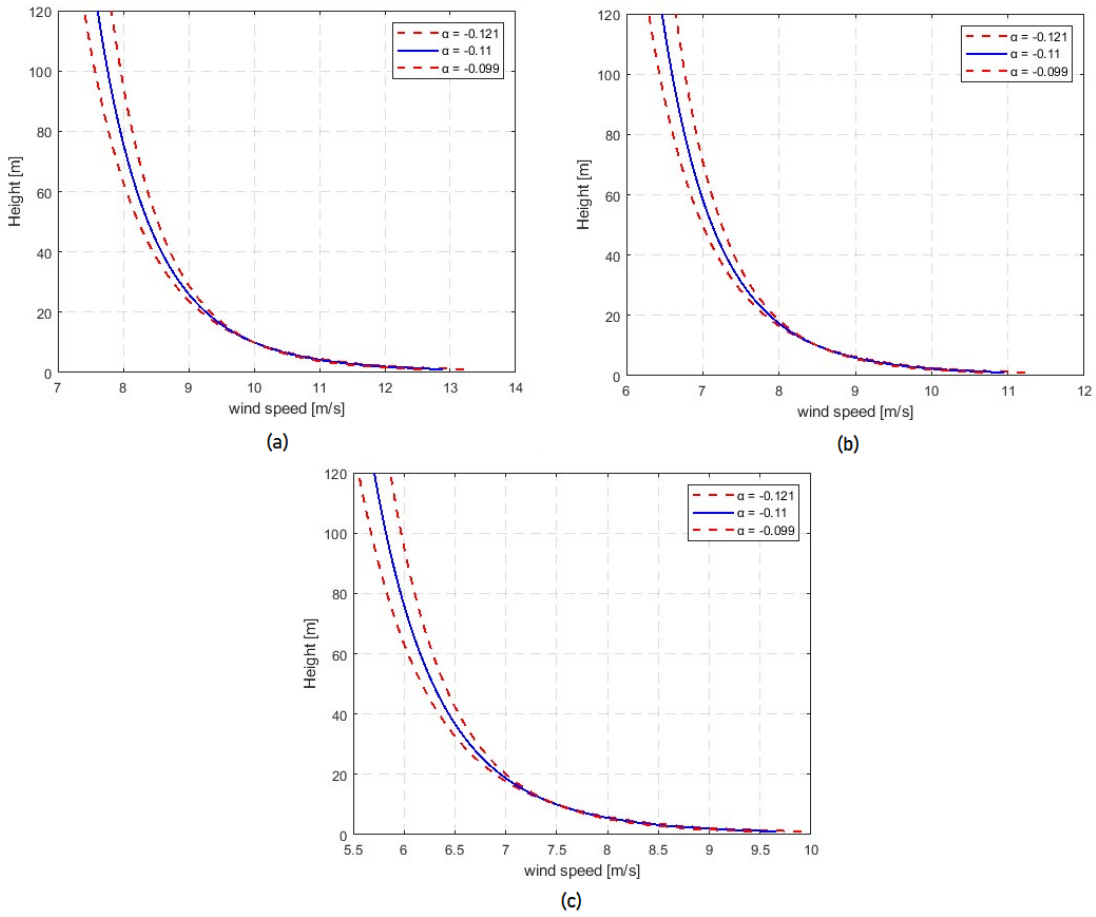

Figure 4.4 Wind speed profile along tower height of 120m with -0.11 wind shear coefficient and %10 margin (a) $v(z_{ref}) = 10\ m/s$, (b) $v(z_{ref}) = 8.5 m/s$, (c) $v(z_{ref}) = 7.5\ m/s$

The results are presented in Figure 4.5 and Figure 4.6 indicate the wind profile between 37m and 120m for the blades below the RNA, and the wind profile between 120m and 203m for the blade above the RNA. Since blade length is 83m, exact solution of a wind profile is created for the blade above the RNA, starting from 120 meters and starting from 37 meters for the blade under the RNA.

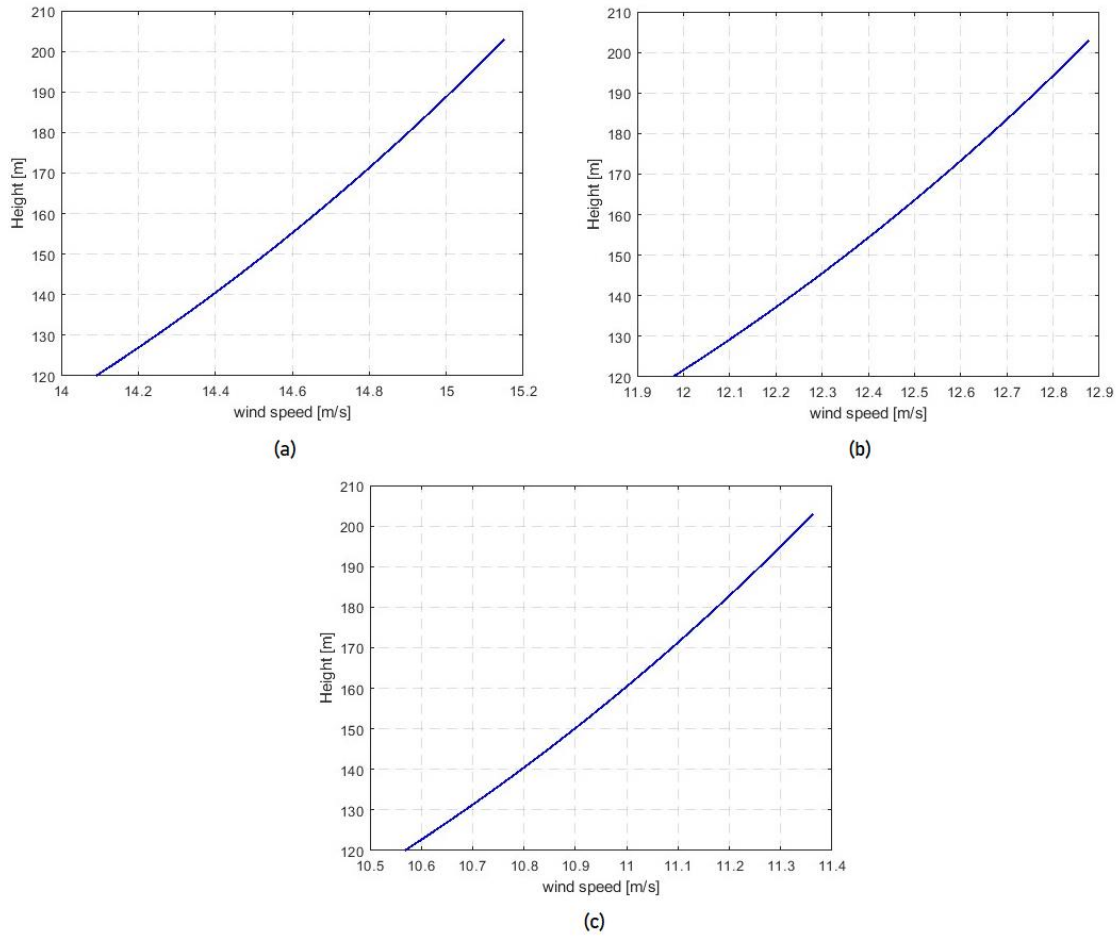

Figure 4.5 Wind speed profile acting on the blade above RNA (a) $v(z_{ref}) = 10\ m/s$, (b) $v(z_{ref}) = 8.5 m/s$, (c) $v(z_{ref}) = 7.5\ m/s$

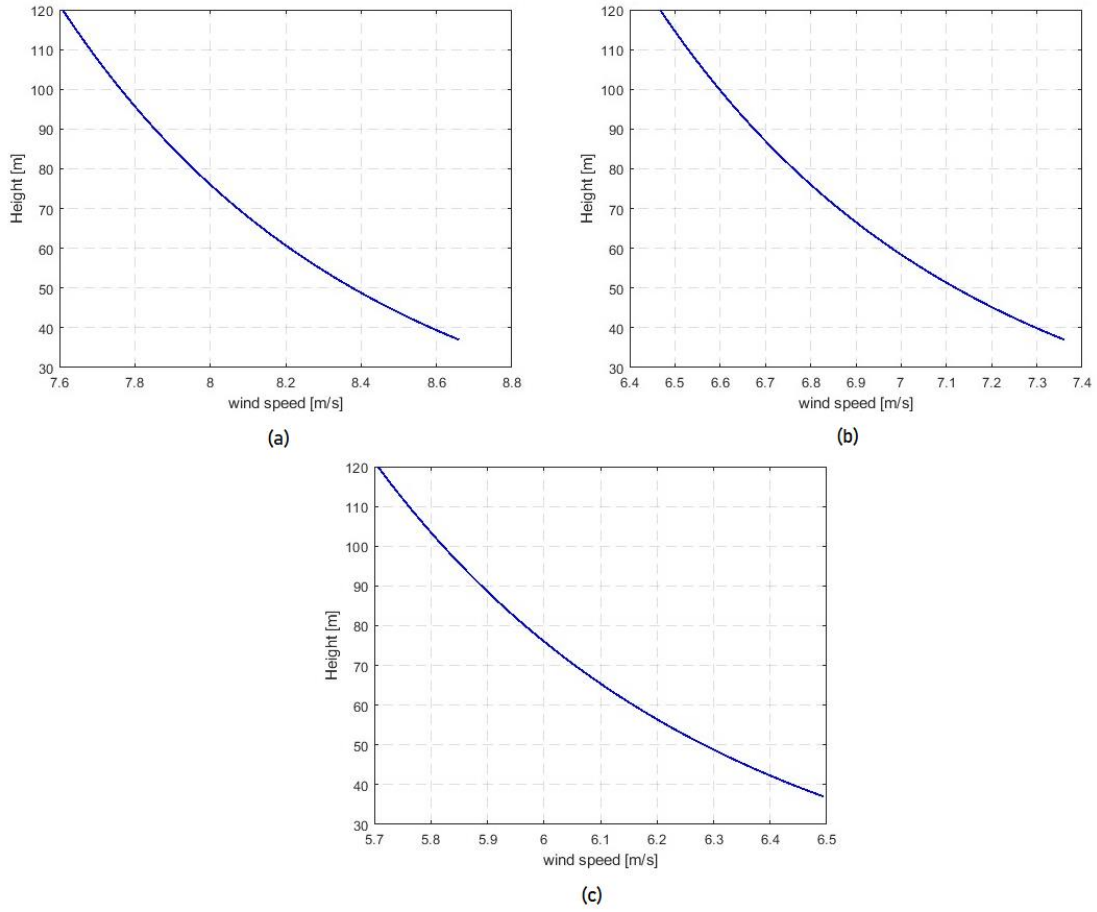

Figure 4.6 Wind speed profile acting on the blade below RNA (a) $\upsilon(z_{ref}) = 10\ m/s$, (b) $\upsilon(z_{ref}) = 8.5 m/s$, (c) $\upsilon(z_{ref}) = 7.5\ m/s$

Although the non-linear power law method is used from the atmospheric boundary layer, which includes wind shear coefficient, which is a complex indicator of wind profiles such as regional climatology, environmental condition, atmospheric stability, it is necessary to take into account the fluctuation of the wind flow along the blade. To obtain the fluctuation of the wind along the blade, the third order (cubic function) equation with coefficients $a_1, a_2, a_3\ and\ a_4$ is adapted to the power law method with curve fitting management for the wind profile function. As mentioned on beam models in chapter 3, beams subjected to a certain load deformation and change in their geometric shapes. After this change, the wind turbine blades, which are modeled as beams, will be stretched, and displaced on the vertical axis. Therefore, while the wind profiles are being created, the wind profiles are updated

in accordance with the new positions of these blades with the curve fitting method. This creates an iterative solution because the first created beam model is located perpendicular to the wind profile, the change in shape after the wind turbine blade is exposed to the wind profile will produce different data for the curve fitting method, and a new function is created by combining these data with the first created wind profile data. Figure 4.7 and Figure 4.8 shows that the velocity values of the wind profile in sections of every 5m on the wind turbine blade both when the wind turbine blade is perpendicular to the profile and after deformation.

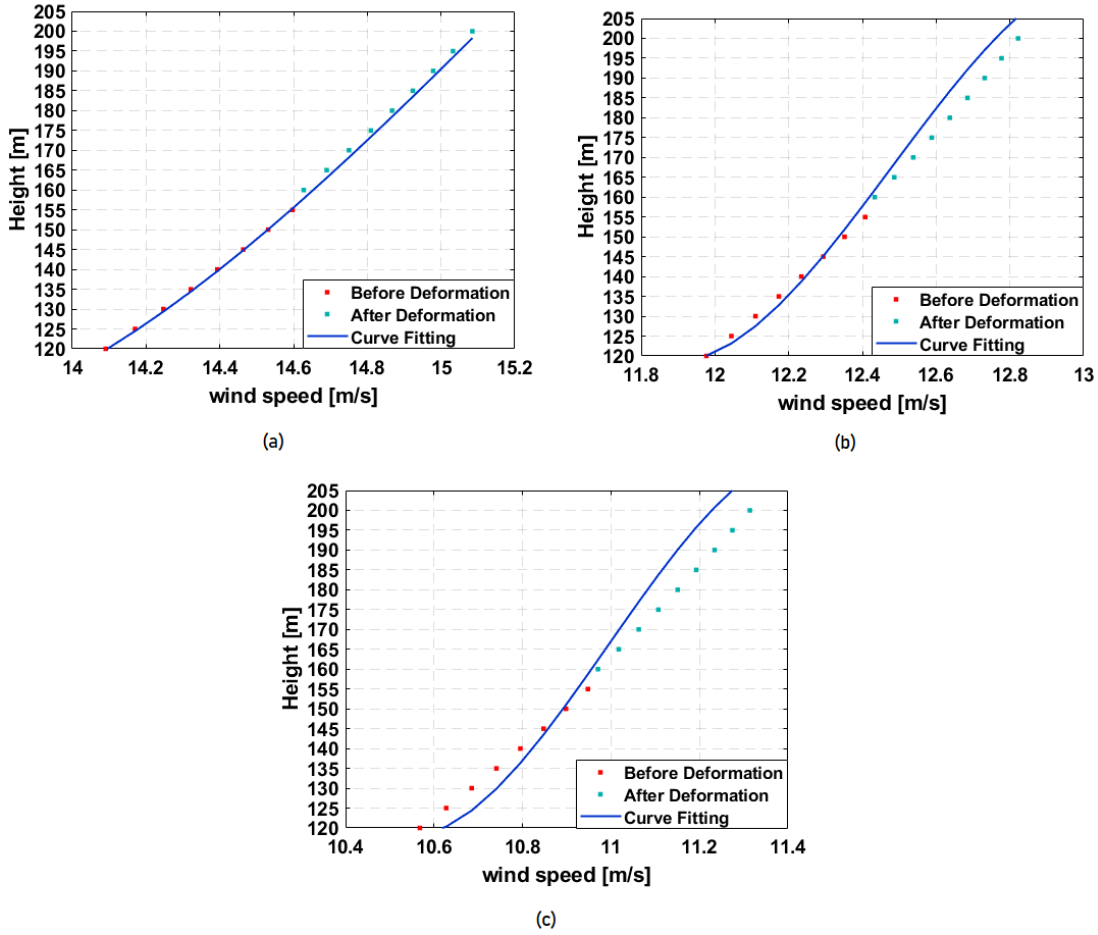

Figure 4.7 Applied curve fitting method to wind speed profile acting on the blade above RNA with 0.138 wind shear coefficient (a) $v(z_{ref}) = 10\ m/s$, (b) $v(z_{ref}) = 8.5m/s$, (c) $v(z_{ref}) = 7.5\ m/s$

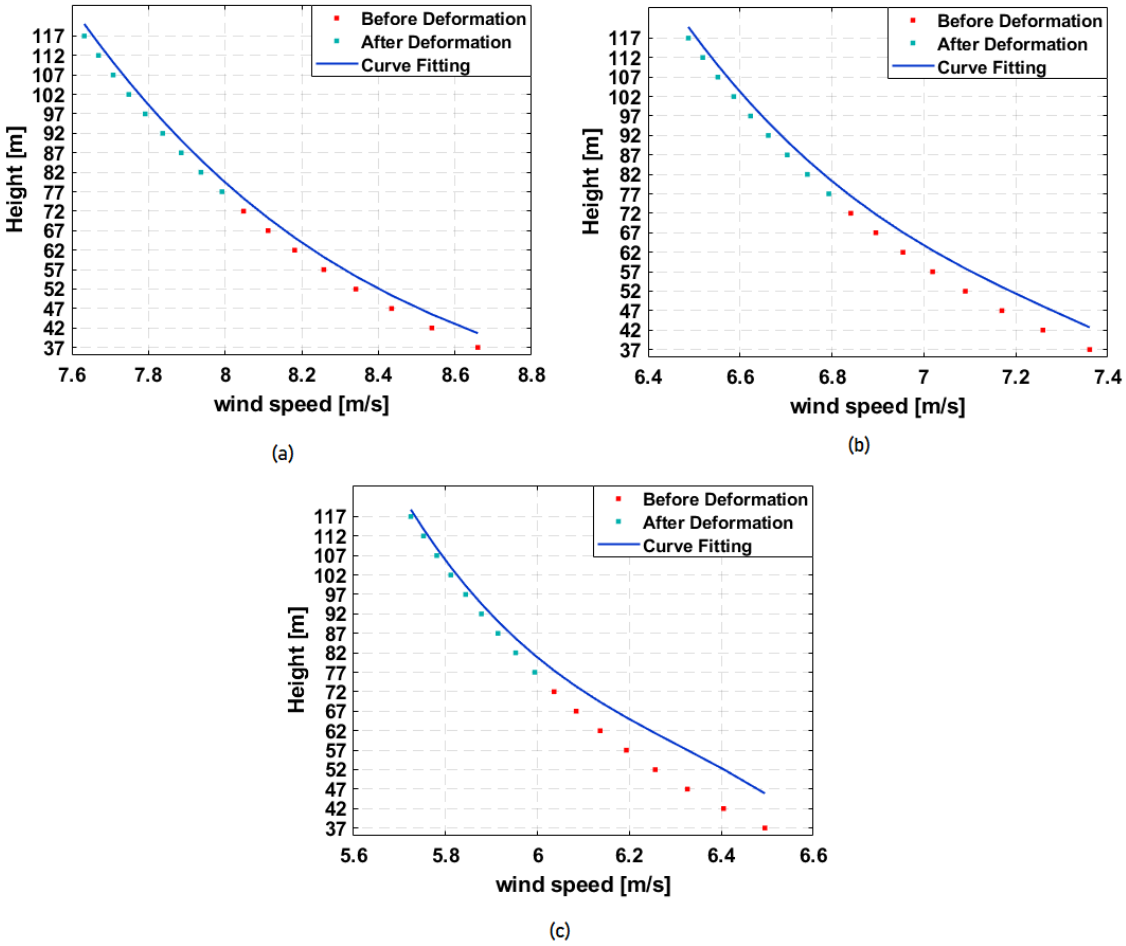

Figure 4.8 Applied curve fitting method to wind speed profile acting on the blade below RNA with -0.11 wind shear coefficient (a) $v(z_{ref}) = 10\ m/s$, (b) $v(z_{ref}) = 8.5 m/s$, (c) $v(z_{ref}) = 7.5\ m/s$

After combining the all data, wind profile is created with curve fitting method. Table 4.2 states the results of coefficient of the third order equation in order of 10 m/s, 8.5 m/s and 7.5 m/s.

Table 4.2 Parameter for wind turbine speed profile from curve fitting

V_{ave} (m/s)	**Wind speed profile acting on the blade above RNA**				**Wind speed profile acting on the blade below RNA**			
	a_1	a_2	a_3	a_4	a_1	a_2	a_3	a_4
10	-8.7529	400.9	-6027.4	29940	-18.196	492.59	-4475.5	13674
8.5	-119.41	4470.6	-55667	230699	-50.038	1101.7	-8138.5	20213
7.5	-262.36	8652.2	-94952	346924	-122.05	2311.1	-14649	31138

As expressed in the Chapter 3, Euler-Bernoulli Beam Model and Timoshenko Beam Model are applied to find the shear forces $V(x)$ and bending moments $M(x)$ from the blades to be used as inputs for the simulations. Successive integration of governing equation is used to reach general solution of $\omega(x)$, $V(x)$ and $M(x)$ for known wind speed profile acting on blades. The requirement of the wind speed profile function is that it is a third-order function to reflect fluctuation of the wind with respect to altitude. The wind speed profile input is defined as non-uniform distributed load, and comparisons are presented with two different beam models when the shaft is rotating at rated wind speed. By application of the boundary condition to the governing equation, bending moment and shear force results for two different beam models are obtained.

Table 4.3 Flexural rigidity values along blade sections

Blade sections (m)	EI (kNm^2)
$0-13$	9865616
$13-26$	3857248
$26-39$	540488
$39-52$	127588
$52-65$	146852
$65-78$	427255
$78-83$	178774

Wind turbine blades are formed in different sections along the blade. EI values (flexural rigidity values) differ due to the structure of these sections with different airfoil types. In order to obtain the shear force and bending moment at the root of the blade more accurately, the blade was divided into 7 different sections using the Abaqus software and the wind load obtained on the blade was applied. The flexural rigidity values that differ along the blade are given in the Table 4.3.

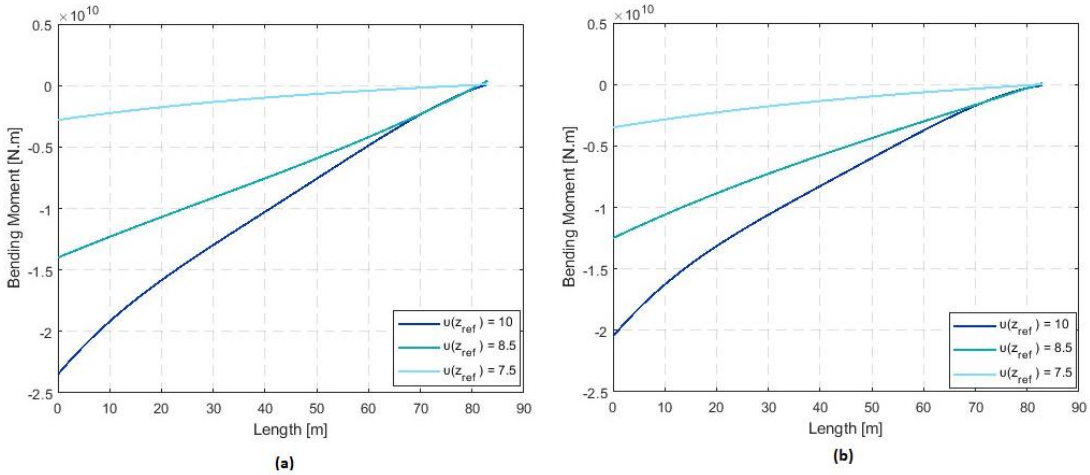

Figure 4.9 Result of bending moment along the blade above RNA (a) using Timoshenko Beam Model (b) using Euler-Bernoulli Beam Model

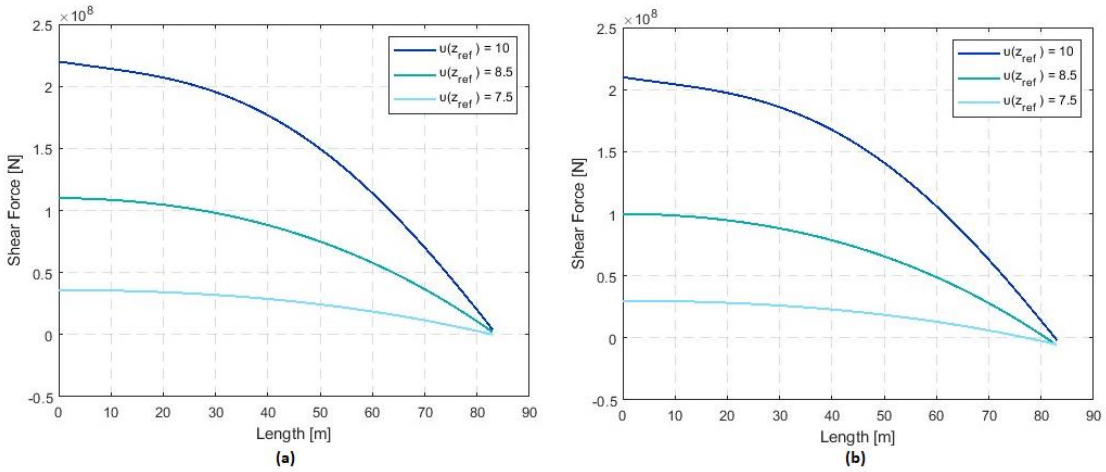

Figure 4.10 Result of shear force along the blade above RNA (a) using Timoshenko Beam Model (b) using Euler-Bernoulli Beam Model

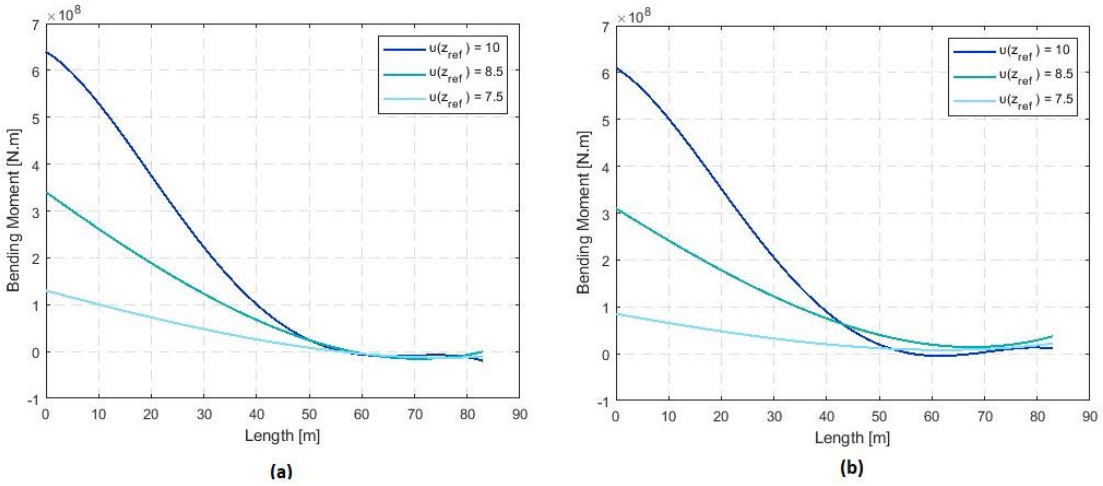

Figure 4.11 Result of bending moment along the blade below RNA (a) using Timoshenko Beam Model (b) using Euler-Bernoulli Beam Model

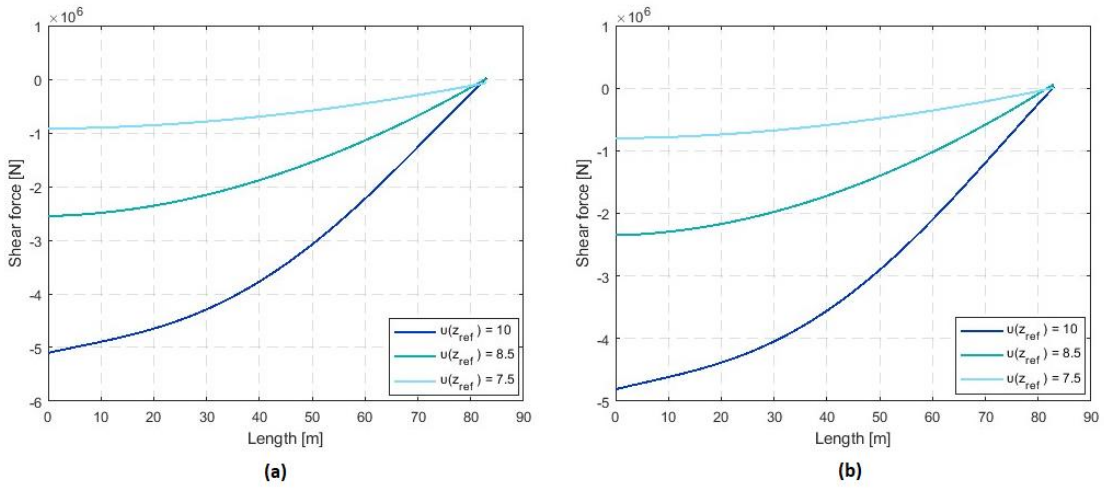

Figure 4.12 Result of shear force along the blade below RNA (a) using Timoshenko Beam Model (b) using Euler-Bernoulli Beam Model

Figure 4.9, Figure 4.10, Figure 4.11 and Figure 4.12 show us that after the wind load effect is applied, there are differences not only in bending moment results but also in shear forces between Euler-Bernoulli Beam Model and Timoshenko Beam Model. Since the wind speed profile is reflected on the blade geometry formed after shear deformation in the Timoshenko beam model and Euler-Bernoulli Beam model, the wind profile function and the beam equation in Equation 3.7 and Equation 3.20 have been updated. For the blade above the RNA, although there is no difference between the Equation 3.2 and Equation 3.18 formulas, there is a difference up to 11 percentage for blades above RNA and 6 percentage for the blade below RNA in the shear forces at the root of the blade due to the influencing wind profile. The reason why the differences of shear forces are higher in the blades above the RNA than in the blade below the RNA will be due to the fact that the created wind profile is more severe for the blades above the RNA and the non-uniformly distributed load in equation Equation 3.7 plays a direct role in the equation. Bending Moment Solutions are shown in Figure 4.9 and Figure 4.11. It is predicted that there will be differences because the beam models under RNA and above RNA use different assumptions. In addition to these assumptions, the difference in the wind profile due to the geometry changes in the Timoshenko beam model and Euler-Bernoulli Beam model also affected the bending moment solutions at the blade root. Since only shear forces and

bending moments at the root of the blade will be used in this study, the percentage changes in the root of the blade are calculated as follows, at above RNA, %11 and %8 for bending moment respectively $v(z_{ref}) = 10\ m/s$ and $v(z_{ref}) = 7.5m/s$, at above RNA, %5 and %4 for shear force respectively $v(z_{ref}) = 10\ m/s$ and $v(z_{ref}) = 7.5m/s$, at below RNA, %6 and %4 for bending moment respectively $v(z_{ref}) = 10\ m/s$ and $v(z_{ref}) = 7.5m/s$, at below RNA, %11 and %6 for shear force respectively $v(z_{ref}) = 10\ m/s$ and $v(z_{ref}) = 7.5m/s$. Furthermore, due to the boundary conditions at the blade root in the beam models, all of the non-uniform distributed load directly affects the blade root. This means that the blade root is stressed region that has the highest shear force and bending moment. According to Timoshenko Beam Model, shear force and bending moment are -5.1e^6 N and 6.4e^8 N.m respectively for wind profile below RNA for $v(z_{ref}) = 10\ m/s$. Moreover, according to Timoshenko Beam Model shear force and bending moment are around 2.3e^8 N and -2.4e^{10} N.m respectively for wind profile above RNA and for $v(z_{ref}) = 10\ m/s$. One of the main purposes of this study is to compare two beam models found in the literature and generally used, but it was predicted that the Timoshenko beam model would be more suitable for blade modeling due to the thickness and length ratio specified in chapter 3 of wind turbine blades being over 1/10. In this comparison, it will be proven again that the shear force and bending moment change rate between beam models has increased up to 11%.

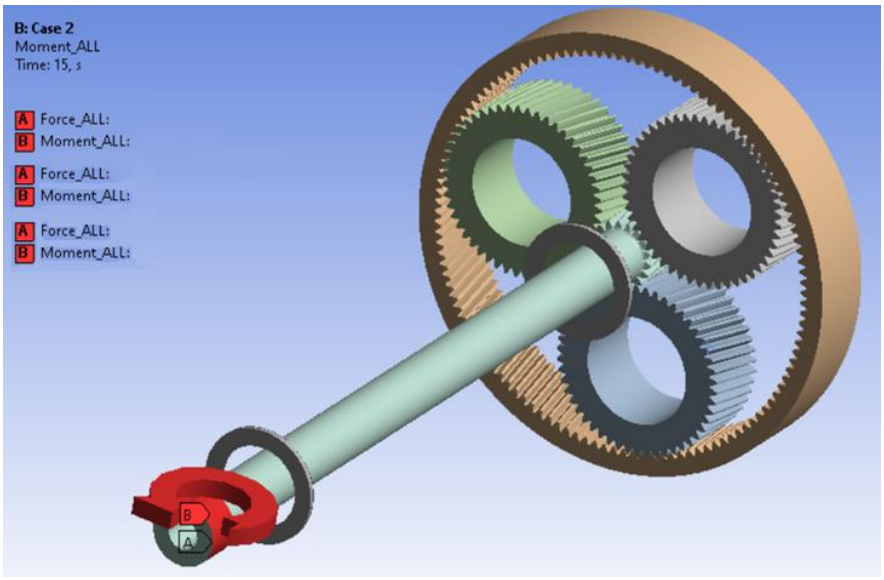

Figure 4.13 Intersection location of blades and shaft

The comparison between Timoshenko beam model and Euler-Bernoulli Beam demonstrated at Figure 4.9 to Figure 4.12. Considering these comparisons, it was decided to run the simulations created with the 3D model by taking the input information from the Timoshenko beam model. The parameters of the simulation setup mentioned in Chapter 3 are the function coefficients of the wind speed profile, the bending moments and shear forces obtained as a result of the analytical analysis created with the Timoshenko beam theory. In addition to the bending moment and shear force from the blades, the weights of the blades were also predicted to affect the simulation results, and the weights of all three blades were added as a point mass in the simulation environment. While running the simulations, three case studies were run in order to observe the variability of the results and to perform a comparison of the case studies for better understanding of effect of the reverse load case. In first case study, the shaft rotates at 8.88 rpm and there is no wind effect from the blade to the shaft. This is the simplest of the load simulations in this study. The second case study is the case that occurs as a result of the generic effect of the wind profile while the shaft rotates with the same rotational speed. In this case, the wind speed profile specified in section 2.1.2.2 was applied uniformly across all blades, and the coefficients of a1, a2, a3 and a4 in the analysis input parameters were utilized. After

this case study, the reverse load condition and the generically generated wind speed profile results were compared. The last case is the effect of the reverse load condition. In order to successfully adapt the reverse load case to the simulation inputs, both the wind speed profile coefficients as well as the shear force and bending moment from the blades are taken from the results section. Finally, in the reverse load case study, the failure types of the gears were investigated under the determined wind speed profiles. By examining the simulation results, it was determined which of these failure types was dominant, namely pitting or bending root cause.

Figure 4.14 Results of SF in the case study of the shaft rotates at 8.88 rpm and there is no wind effect from the blade to the shaft

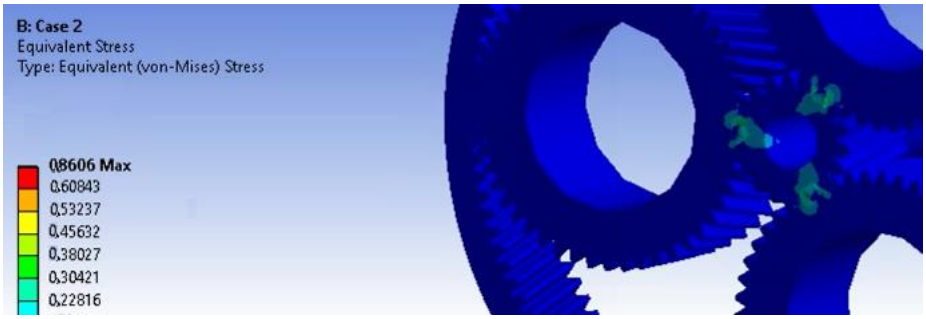

Figure 4.15 Results of SF in the case study of the shaft rotates at 8.88 rpm and generic effect of the wind profile from the blade to the shaft

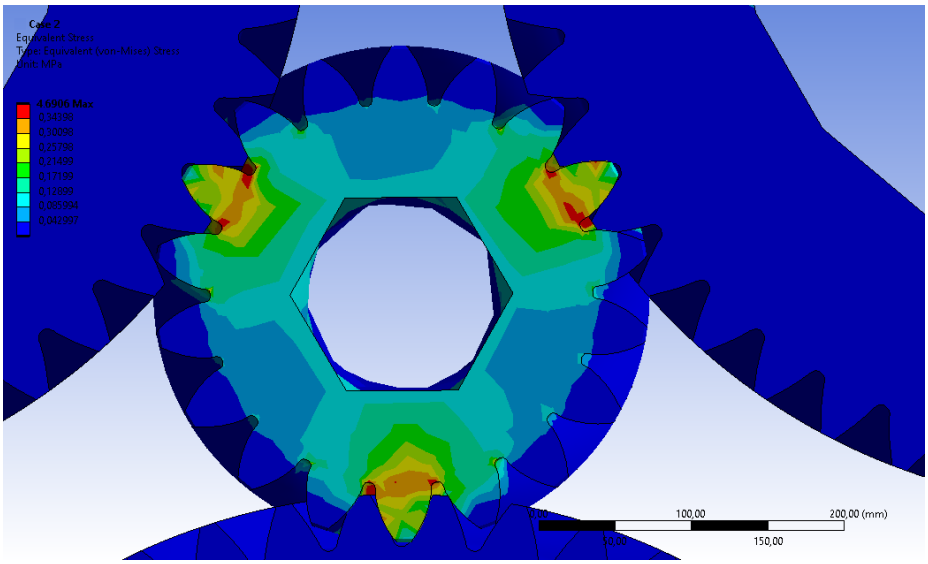

Figure 4.16 SF von-Misses results for the most critical condition “reverse load condition”

From the finite element simulation results, von Mises failure criteria is considered in order to determine the critical area for failure according to specified material strength data. Basically, von Mises criteria combines principal stresses on the structure (σ1, σ2, σ3) with the compressive strength (CS) and tensile strength (TS) of the material to obtain a safety factor (SF). Therefore, critical regions can be determined when the material strength data and von Mises stress values are correlated as SF over the software. If safety factor values lower than unity, material is in safe zone. However, if values greater than unity, this implies that the material is prone to have a mechanical failure. Figure 4.14, Figure 4.16 and Figure 4.16 show that the von Mises stress values are limited to SF according to the material strength at three different loading conditions. In this figure, color scale is fixed to unity and parts above unity are shown in red color.

We can understand from Figure 4.14 and Figure 4.15 that when we compare the stress values generated as a result of the simulations over the corresponding material yield stress, there is no value above unity. However, as seen in Figure 4.16, after the von Mises stress values formed as a result of the simulation are divided by the yield

stress value of the material, the regions visualized in red are seen above unity as the SF factor.

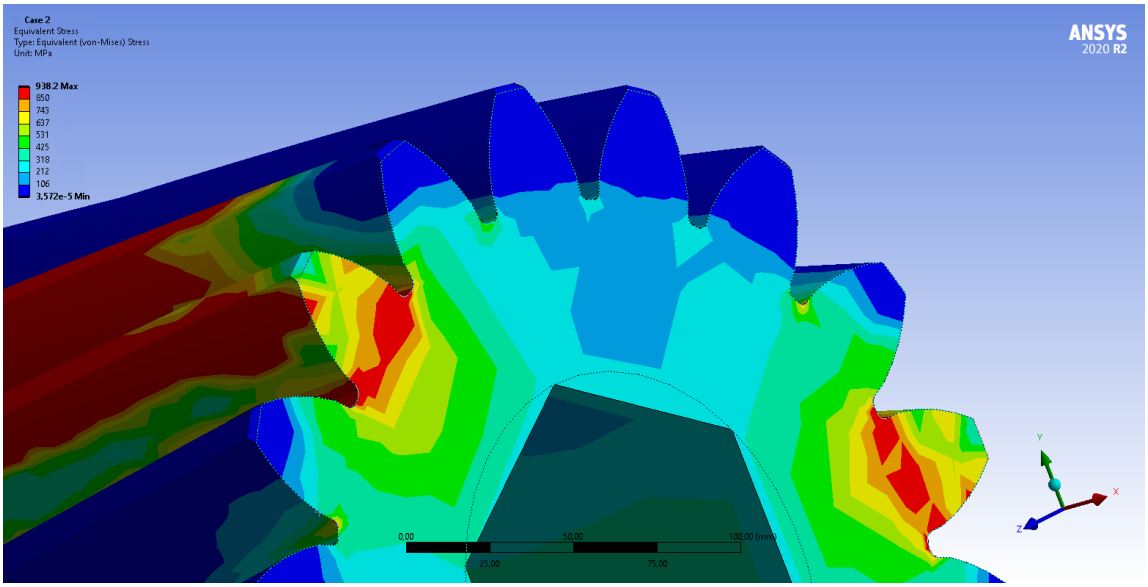

Figure 4.17 Results of von Mises stress in the case study of reverse load condition for sun gear

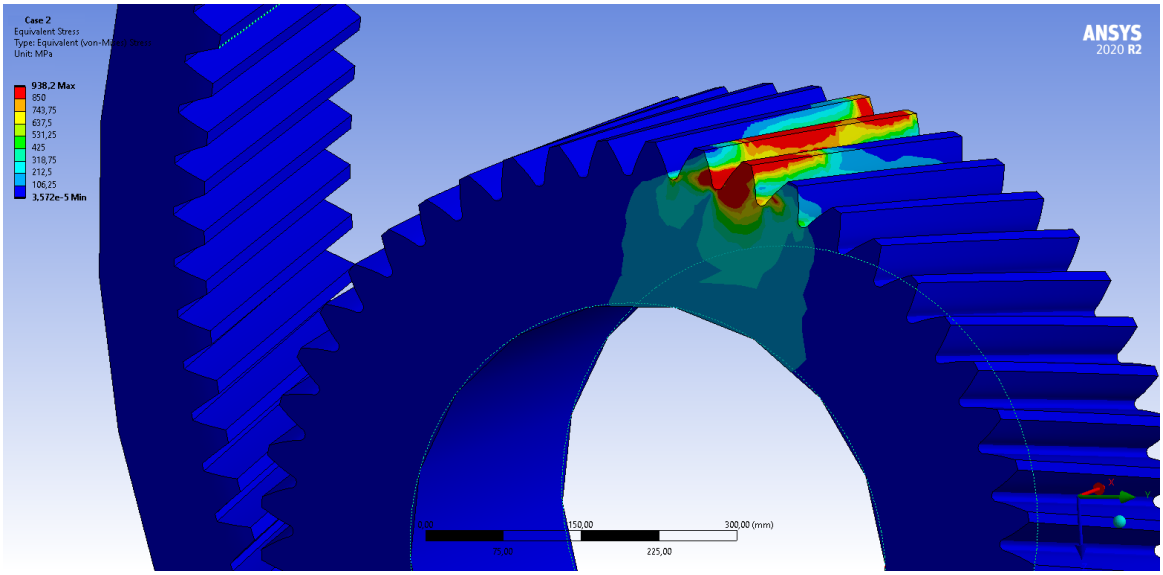

Figure 4.18 Results of von Mises stress in the case study of reverse load condition for planet gear

The distribution of von Mises stress values on both the planet gear and the sun gear are displayed and examined. These distributions show us the propagation of stress values on the structure. By using the finite element model, the locations that may fail on the three-dimensional structures are determined. In Figure 4.17, the stress values on the sun gear are given and the visual labeling is fixed at 850 MPa that is the point where the material will leave the elastic region and fall under the plastic region. It is observed that the propogation of the stress will be in the root part of the gear. In Figure 4.18, the same visual labeling was made on the planetary gear and the values above 850 MPa were taken into account, and considering the reverse load situation, it was determined that the distribution of the propagation on the gear root would be more critical than the propagation on the gear tooth surface. Singularity at the contact points are not taken into account. The stress values on the gears as a result of these judgments, regardless of a general rule, are shown Figure 4.17 and Figure 4.18. The time dependent variation of the stress history on three different planet gears is shown in Figure 4.19. Considering the results, the stress values examined for the determination of the failure mechanism were achieved by considering the stress intensity at the maximum level. In addition, the results at the moment when the stress intensity is maximum were examined for both planetary gears and sun gears.

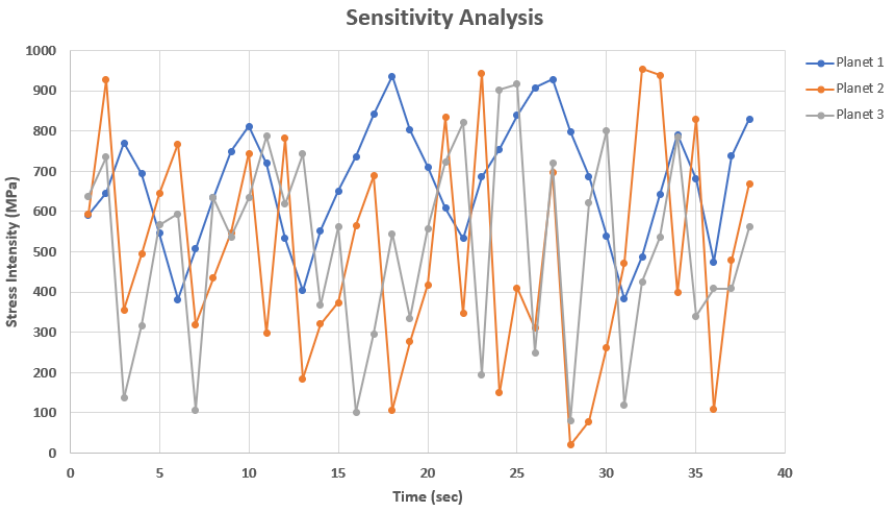

Figure 4.19 The stress intensity for planet gears

CHAPTER 5

CONCLUSION & FUTURE WORK

For more than a century, many researchers have been working on gears that look like a simple mechanism but have a complex structure. Although many modeling methods are used in the literature for gearboxes, the planetary gear set in wind turbines requires improvement due to the fact that it works for a very long time in operation, or because it is exposed to the wind load that varies too much. As the scope of this study, a different modeling method has been presented and the failure types of the gears in the wind turbine gear set have been determined. Since the importance level of the components inside the turbine may differ depending on the wind load, the most critical wind condition was determined for the gear set and two different beam models were compared for this wind condition. Overall, it has been observed that the comparisons between the beam models and the information in the standards while creating the wind speed profile are compatible. A new loading condition has been established for wind turbine gear sets as a result of the examinations between the cases with design limits in the literature and standards. The name of this loading condition is reverse load condition. For this loading condition, the wind speed profile should be specially prepared and applied to the new model. In order to see the effect of the obtained wind speed profile, the modeling results of the generically prepared wind speed profiles in the standards were compared. It is understood from these results that the reverse loading condition creates more critical loads for the gears. Wind turbine blades are developing with new technologies and their length is increasing. The main reasons is to collect the energy from the wind in a larger area and to increase efficiency. Therefore, modeling of wind turbine blades becomes challenging with innovations. The main reason for using two different beam models in this study is to observe the difference between beam models to enrich the study and to provide more accurate modeling of turbine

blades with increasing length. The difference between the two beam models used is due to the inertia effect, shear deformation being taken into account, and shear deformation is effective in structures with a length-to-thickness ratio less than 1/10. Considering the wind turbine blades, it has been observed that the beam model, which takes into account shear deformation, will be more compatible. In addition to obtaining a critical loading scenario and comparing beam models, three different simulation setup were performed. These simulations are used to determine gear failure type. In conclusion, reverse load condition causes the bending moment failure at the gear root rather than the pitting on the gear tooth surface under specified wind load according to simulation results.

As a discussion point, both the theoretical and experimental results of the wind turbine failure mechanisms in the literature were examined and the researches were compared with the results of this thesis. For example, Gang, Dong, Kan, Li, Yinhua and Yalin states that by analyzing the actual failing components, the fretting wear morphology and visible micro cracks can be found on the inner surface of planetary gear. Based on their investigation, they classified the failure developing process of planetary gears with two different stages, fretting wear and source generation in their study. In both stages, they come up with the conclusion of concentrated stress eventually leads to the generation of failing source [45]. Therefore, understanding whether the stress concentration on the gears will occur at the gear surface or at the gear root plays a crucial role in reaching the source of the failure type. Another discussion point is that there may be negotiation between material update solutions or geometry-based solutions, for example rim thickness. Because the source of failure varies between components due to different loading scenarios, and the solution of this failure can be solved by both material changes and geometry-related changes depending on the failure source.

This thesis proposes a few guidelines for wind turbine gear train designers;

- Since the probability of failure of components inside the wind turbine can vary depending on wind load, the most critical wind condition for the gear train must be determined. For example, Reverse Load Condition, the wind speed profile must be specially prepared and applied to the model.

- The failure mechanisms of the gear sets on the gear train should be determined. For example, according to this thesis, the failure mechanism for reverse load condition is the bending moment at the root of gear tooth. In addition, precautions should be taken against the loading scenario that causes these failure mechanisms. Design changes or material changes can be an example.

- Gear box type should be determined by considering the most extreme loading conditions that may occur. For example, 3-planet gear, 4-planet gear configurations play an important role in sharing the stresses that may occur during loading and relieving the loads on the gear, so the choice of gearbox type should be examined by the designers.

For the further investigations, verifying and validating results with existing turbine data is essential for wind speed profile estimation. Without validation, the significance of the data lacks confidence. Turbine data with similar data can be examined to observe potential wind patterns that may be subject to reverse loading. In addition, improvements can be made on the model used, for example, the boundary conditions used in the simulations were determined from the part of the shaft with the bearings, but these boundary conditions can be created with a different support setup and a more realistic model can be obtained.

REFERENCES

[1] "The economics of wind energy" vol. 9, European Wind Energy Association (EWEA), 2009.

[2] "Global Wind 2009 Report: Market forecast 2010-2014," *Global Wind Energy Council (GWEC), Brussels, Belgium*, 2010.

[3] "Wind energy in Europe: Scenarios for 2030," September, 2017.

[4] "Global Energy Transformation: A Roadmap to 2050," International Renewable Energy Agency (IRENA), 2018.

[5] "Wind power in Turkey: Vestas wind turbines for a wind farm," May, 2015.

[6] R. Ata, "The Current Situation of Wind Energy in Turkey," *in Hindawi Journal of Energy*, 2013.

[7] Al-Hamadani, Haider Rahman Dawood. "System Dynamic Modelling of Wind Turbine Gearbox Under Normal and Transient Operating Conditions." PhD diss., University of Sheffield, 2018.

[8] K Scott, Kenneth. "Effects of transient loading on wind turbine drivetrains." 30th ASME Wind Energy Symposium, Nashville, USA, 2014

[9] Bartelmus, Walter, Fakher Chaari, Radoslaw Zimroz, and Mohamed Haddar. "Modelling of gearbox dynamics under time-varying nonstationary load for distributed fault detection and diagnosis." European Journal of Mechanics-A/Solids 29, no. 4 (2010): 637-646.

[10] Rassokha, Vladimir, and Vladimir Isaychev. "New design of the automobile automatic gearbox providing driving simplification and driver fatigue decrease." Transportation Research Procedia 20 (2017): 544-549.

[11] Guo, Yi, and Robert G. Parker. "Dynamic modeling and analysis of a spur planetary gear involving tooth wedging and bearing clearance nonlinearity." European Journal of Mechanics-A/Solids 29, no. 6 (2010).

[12] Chaari, Fakher, Tahar Fakhfakh, and Mohamed Haddar. "Analytical modelling of spur gear tooth crack and influence on gearmesh stiffness." European Journal of Mechanics-A/Solids 28, no. 3 (2009).

[13] Chen, Xianhua. "Dynamic Model of a Planetary Gearbox considering Sun Gear Crack with Effects of Clearance for Carrier, Planet and Sun Gear Bearings." (2020).

[14] Liang, Xihui, Ming J. Zuo, and Mohammad R. Hoseini. "Vibration signal modeling of a planetary gear set for tooth crack detection." Engineering Failure Analysis 48 (2015).

[15] Liang, Xihui, Ming J. Zuo, and Tejas H. Patel. "Evaluating the time-varying mesh stiffness of a planetary gear set using the potential energy method." Proceedings of the Institution of Mechanical Engineers, Part C: Journal of Mechanical Engineering Science 228, no. 3 (2014): 535-547.

[16] Díaz, Matías, Roberto Cardenas, B. Mauricio Espinoza, Andrés Mora, and Félix Rojas. "A novel LVRT control strategy for modular multilevel matrix converter based high-power wind energy conversion systems." In 2015 Tenth International Conference on Ecological Vehicles and Renewable Energies (EVER), pp. 1-11. IEEE, 2015.

[17] S. Sheng, "Wind turbine gearbox condition monitoring round robin study – vibration analysis," National Renewable Energy Lab.(NREL), (2012).

[18] Uraz, Emre. "Offshore wind turbine transportation & installation analyses planning optimal marine operations for offshore wind projects." (2011).

[19] Anonymous, "Gearboxes-the Achilles heel of wind power engineering (Special Focus Article)," Windpower Monthly, vol. 21, (2005).

[20] W. Musial, S. Butterfield, and B. McNiff, "Improving wind turbine gearbox reliability: preprint," National Renewable Energy Lab.(NREL), Golden, CO United States (2007).

[21] Grujicic, M., S. Ramaswami, J. S. Snipes, R. Galgalikar, V. Chenna, and R. Yavari. "Computer-aided engineering analysis of tooth-bending fatigue-based failure in horizontal-axis wind-turbine gearboxes." International Journal of Structural Integrity (2014).

[22] Helsen, Jan, Frederik Vanhollebeke, Dirk Vandepitte, and Wim Desmet. "Some trends and challenges in wind turbine upscaling." In Proceedings of ISMA International Conference On Noise And Vibration 2012, vol. 6, pp. 4345-4359. 2012.

[23] Wei, J., et al., "A study on optimum design method of gear transmission system for wind turbine. International Journal of Precision Engineering and Manufacturing." (2013): pp. 767-778.

[24] Akinnuli, B., T. I. Ogedengbe, and K. O. Oladosu. "Computer aided design and drafting of helical gears." J. Eng. Trends Appl. Sci 3 (2012): 959-968.

[25] S. Burton, Jenkins, Bossanyi, Wind Energy Handbook, 2001.

[26] Davenport, A. G. "The prediction of the response of structures to gusty wind." Safety of structures under dynamic loading 1 (1977): 257-284.

[27] "The EU offshore renewable energy strategy." Wind Europe, 2020.

[28] S. Vorrath, Renewable economy Handbook, 2020.

[29] Harris, R.I. "The nature of wind in the modern design of wind-sensitive structures". London: Construction Industry Research and Information Association, (1971).

[30] Mukherjee, R., Mohammadi, M.S. "Wind Loads in Bridges," 2013, pp 11.

[31] Davenport, Alan G. "The response of slender, line-like structures to a gusty wind." Proceedings of the Institution of Civil Engineers 23, no. 3 (1962).

[32] Davenport, Alan G. "Gust loading factors." Journal of the Structural Division 93, no. 3 (1967): 11-34.

[33] International Electrotechnical Committee IEC 61400-3: Wind Turbines Part 3: Design Requirements for Offshore Wind Turbines; 1st ed.; IEC: Geneva, Switzerland, 2009

[34] Paul S Veers, Sandy Butterfield, "Extreme Load Estimation for Wind Turbines: Issues and Opportunities for Improved Practice," National Wind Technology Center National Renewable Energy Laboratory, 2001.

[35] Haver, S., "Application of Stochastic Methods in Structural Design The Offshore Experience." A collection of the 2001 ASME Wind Energy Symp, January 2001.

[36] Veers, Paul S., and Steven R. Winterstein. "Application of measured loads to wind turbine fatigue and reliability analysis." Journal of Solar Energv Engineering Trans. of the ASME, (1998).

[37] Ronold, Knut O., and Gunner C. Larsen. "Variability of extreme flap loads during turbine operation." In EWEC-CONFERENCE, pp. 107-229. 1999.

[38] Gasch, R.; Twele, J. Wind Power Plants; Solarpraxis: Berlin, Germany, 2002.

[39] Stephen H. Crandall and Norman C. Dahl, et al., An Introduction to The Mechanics of Solids, 2 nd Edition, Mcgraw Hill, 1978.

[40] Wang, C. M., Junuthula Narasimha Reddy, and K. H. Lee, eds. "Shear deformable beams and plates: Relationships with classical solutions. Elsevier." (2000).

[41] Timoshenko, S. P., and J. M. Gere. "Theory of elastic stability (McGraw-Hill Book Company Inc., New York, Toronto, London." (1961)

[42] Cowper. "The shear coefficient in Timoshenko's beam theory." (1966): 335-340.

[43] Bäker, Martin. "How to get meaningful and correct results from your finite element model." (2018).

[44] Singh, Pradeep Kumar, Manwendra Gautam, and Shyam Bihari Lal. "Stress analysis spur gear design by using ANSYS workbench." (2014).

[45] Shen, Gang, Dong Xiang, Kan Zhu, Li Jiang, Yinhua Shen, and Yanlin Li. "Fatigue failure mechanism of planetary gear train for wind turbine gearbox." (2018).

APPENDICES

A. Euler-Bernoulli Beam Solution

From the solution of Equation 3.2 and 3.3

$$\frac{d}{dx}\left(E\mathrm{I}\frac{d^2\omega}{dx^2}\right) = \int^{x} q(\xi)d\xi + c_1 = -V(x) \tag{3.2}$$

$$E\mathrm{I}\frac{d^2\omega}{dx^2} = \int^{x}\int^{\xi} q(\eta)d\eta d\xi + c_1 x + c_2 = -M(x) \tag{3.3}$$

Therefore, "EI" can be considered as constant, then,

$$E\mathrm{I}\frac{d\omega}{dx} = \int^{x}\int^{\xi}\int^{\eta} q(\zeta)d\zeta d\eta d\xi + c_1\frac{x^2}{2} + c_2 x + c_3 \tag{3.4}$$

$$E\mathrm{I}\omega(x) = \int^{x}\int^{\xi}\int^{\eta}\int^{\zeta} q(\mu)d\mu d\zeta d\eta d\xi + c_1\frac{x^3}{6} + c_2\frac{x^2}{2} + c_3 x + c_4 \tag{3.5}$$

Where constants such as $c_1, c_2, c_3\ and\ c_4$ can be integrated to obtain using the boundary conditions of type of supports.